Cenozoic deformation of Iberia: A model for intraplate mountain building and basin development based on analogue modeling

J. Fernández-Lozano,[1,2] D. Sokoutis,[1] E. Willingshofer,[1] S. Cloetingh,[1] and G. De Vicente[2]

Received 7 April 2010; revised 2 September 2010; accepted 23 September 2010; published 8 January 2011.

[1] Inferences from analogue models support lithospheric folding as the primary response to large-scale shortening manifested in the present day topography of Iberia. This process was active from the late Oligocene-early Miocene during the Alpine orogeny and was probably enhanced by reactivation of inherited Variscan faults. The modeling results confirm the dependence of fold wavelength on convergence rate and hence the strength of the layers of the lithosphere such that fold wavelength is longest for fast convergence rates favoring whole lithosphere folding. Folding is associated with the formation of dominantly pop-up type mountain ranges in the brittle crust and thickening of the ductile layers in the synforms of the buckle folds by flow. The mountain ranges are represented by upper crustal pop-ups forming the main topographic relief. The wavelengths of the topographic uplifts, both, in model and nature suggest mechanical decoupling between crust and mantle. Moreover, our modeling results suggest that buckling in Iberia took place under rheological conditions where the lithospheric mantle is stronger than the lower crust. The presence of an indenter, inducing oblique shortening in response to the opening of the King's Trough in the north western corner of the Atlantic Iberian margin controls the spacing and obliquity of structures. This leads to the transfer of the deformation from the moving walls towards the inner part of the model, creating oblique structures in both brittle and ductile layers. The effect of the indenter, together with an increase on the convergence rate produced more complex brittle structures. These results show close similarities to observations on the general shape and distribution of mountain ranges and basins in Iberia, including the Spanish Central System and Toledo Mountains. **Citation:** Fernández-Lozano, J., D. Sokoutis, E. Willingshofer, S. Cloetingh, and G. De Vicente (2011), Cenozoic deformation of Iberia: A model for intraplate mountain building and basin development based on analogue modeling, *Tectonics*, *30*, TC1001, doi:10.1029/2010TC002719.

1. Introduction

[2] The Iberian Peninsula represents the westernmost edge of the continental part of the Eurasian plate. The actual distribution of mountain ranges has been linked to the convergence between the African and European plates during the Cenozoic as documented by deformation along its plate boundary; that is, the Pyrenean stage and the plate interior [*De Vicente and Vegas*, 2009]. Convergence during the late Oligocene led to collision giving rise to mountain uplift and deformation of the Cantabrian-Pyrenean belt [*Martín-González and Heredia*, 2008]. The oldest non-deformed rocks in the Pyrenees are Pliocene and late Miocene in age on the north and southern margin, respectively [*Mattauer and Henry*, 1974, and references therein]. In addition, high topography is present in the peninsula interior and the Betics, which at the same time can be seen as the last increment (last 11 Myr) of mountain building in Iberia (see Figures 1a and 1b).

[3] Models attempting to explain the reoccurrence of significant topography over distances of several hundreds of kilometers in Iberia invoke buckling of the lithosphere [*Cloetingh et al.*, 2002] or isostatic response to crustal thickening [*Casas-Sainz and de Vicente*, 2009], block rotation and uplift [*Vegas et al.*, 1990] or the interaction of several processes regarding thickening and uplift during the main episode of convergence and subsequent stretching by back-arc extension in the Mediterranean [*Vergés and Fernández*, 2006]. Among the above mentioned processes folding of the continental lithosphere has been suggested to be an efficient mechanism that leads to mountain building and general uplift and subsidence [*Stephenson et al.*, 1990; *Doglioni et al.*, 1994; *Burov et al.*, 1993]. The stability of such structures has been estimated to be in the order of 20 Myr maintaining the Moho isotherms relatively stable during most of the life span of such folds [*Cloetingh et al.*, 1999]. Subsequently, the folded lithosphere may be subject to gravity driven deformation-like collapse or lateral extrusion of lower crustal material as proposed by *Bird* [1991], *Rey and Vanderhaeghe* [2001], *Cloetingh et al.* [1999], *Burg et al.* [1997], and *Burov and Watts* [2006].

[4] In order to gain insight into the feasible processes that lead to the distribution of topography and uplift in intra-

[1]Netherlands Research Centre for Integrated Solid Earth Science, Faculty of Earth and Life Sciences, VU University, Amsterdam, Netherlands.
[2]Departamento de Geodinámica, F.C. Geológicas, Universidad Complutense de Madrid, Madrid, Spain.

0278-7407/11/2010TC002719

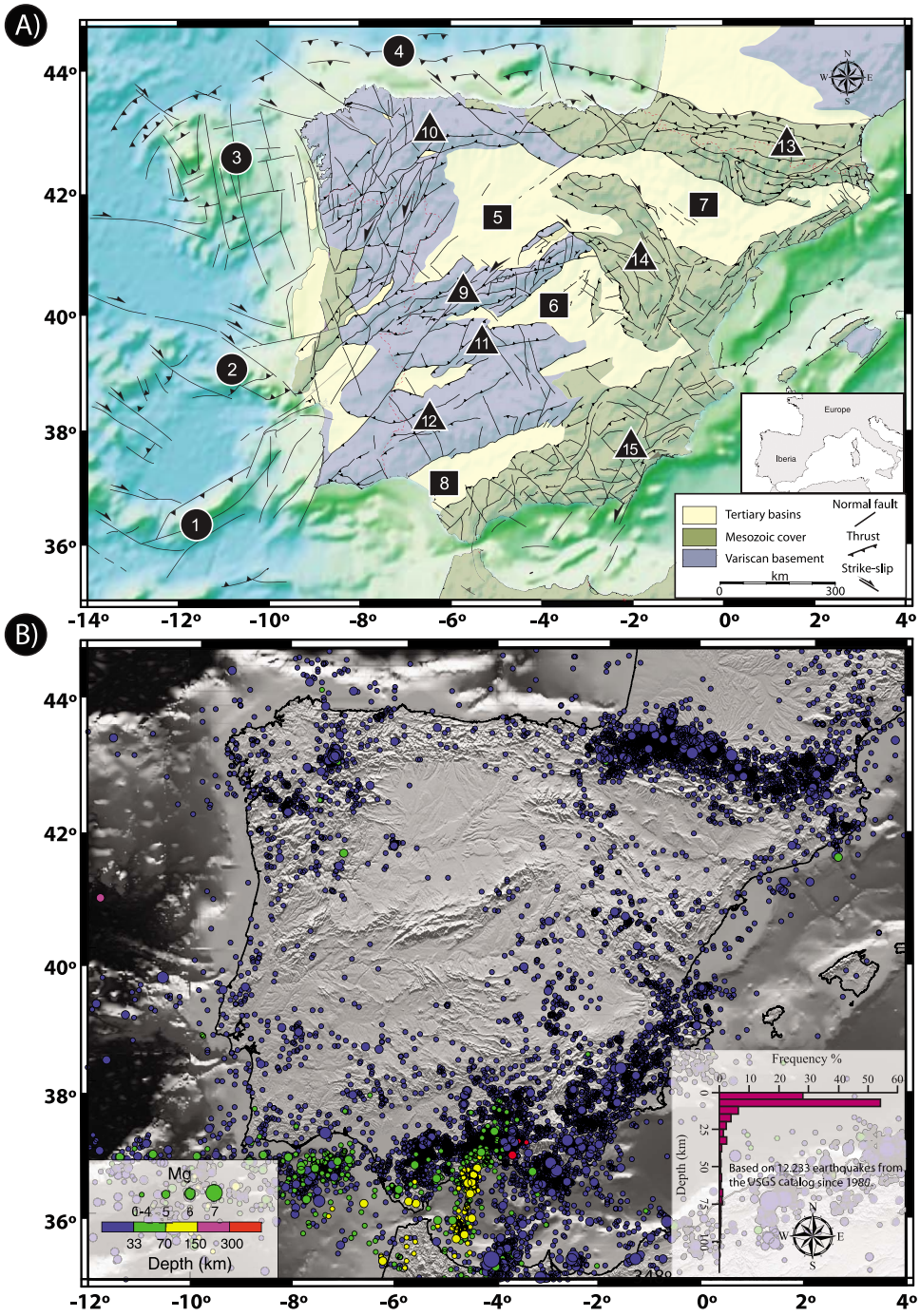

Figure 1. (a) Simplified geological and structural map of Iberia showing the main tectonic fabric. Circles indicate main features offshore: 1, Gorringe Bank; 2, Extremadura Spur; 3, Galicia Bank; 4, Gulf of Biscay. Squares indicate main basins: 5, Duero Basin; 6, Tagus Basin; 7, Ebro Basin; 8, Guadalquivir Basin. Triangles indicate main mountain ranges: 9, Spanish Central System; 10, Cantabrian Mountains; 11, Guadalupe-Montanchez Sierras and Toledo Mountains; 12, Sierra Morena; 13, Pyrenees; 14, Iberian Chain; 15, Betics. (b) Seismicity map of Iberia illustrating earthquake epicenters between 1980 and 2010 (data from U.S. Geological Survey available at http://earthquake.usgs.gov/earthquakes/eqarchives/epic/). Frequency plot indicates the distribution of seismic activity in depth. Markedly interesting is that most of the seismicity is located at a 10 km depth within the plate interior.

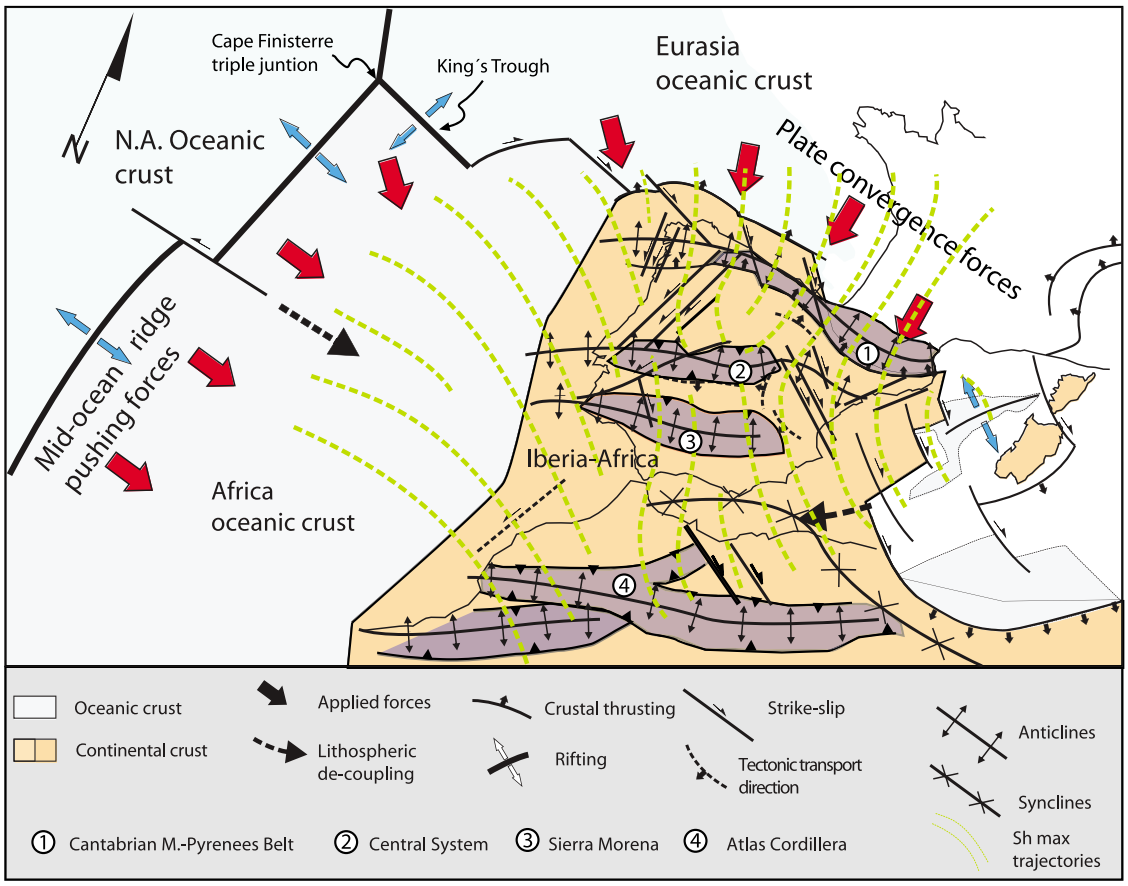

Figure 2. Paleoreconstruction of plate configuration during Oligocene–lower Miocene times showing the main active acting forces and Sh_{max} trajectories modified after *De Vicente and Vegas* [2009]. The circles represent the main intraplate mountain systems for Iberia and northern Africa.

continental lithosphere, a series of analogue models have been conducted. In this study we have tested parameters that could control the wavelength of the folding but also the style of deformation within the upper and lower crust. As such we varied the strength of lithosphere layers and the geometry of the advancing wall because the latter influences the transfer of strain into the plate interior. Consequently, these models allow us to better understand the effect of the rheological stratification and geometrical boundary conditions on deformation of the continental lithosphere in intraplate settings. The Cenozoic tectonic and topographic evolution of Iberia is used to demonstrate the relevance of our modeling results for natural systems.

2. Cenozoic Deformation and Plate Reorganization

[5] From Permian to Triassic times the tectonic setting of Iberia has changed to mainly extensional and the northern Iberian continental margin underwent rifting during Late Jurassic-Early Cretaceous times [*Álvarez-Marrón et al.*, 1996]. During this time, the Cape Finisterre triple point was active leading to an opening along the Palmer ridge, which was created 60 Myr ago in the NE Atlantic. The Palmer ridge opening led to uplift and spreading along the "King's Trough" (Figure 2) about 27 Myr ago [*Cann and Funnell*, 1967]. Paleomagnetic data from sediments of the Lusitanian basin and the Algarve [*Márton and Abranches*, 2004], indicate a 26° counterclockwise rotation of Iberia produced by the opening of the Bay of Biscay during the Late Cretaceous. Rotation was accommodated along major left-lateral strike-slip faults without any evidence of earlier and additional counterclockwise rotation during the Cretaceous. After Late Cretaceous time, Iberia remained attached (mechanically coupled, *Vegas* [2005]) to the African Plate until the late Eocene.

[6] From Eocene to late Oligocene times, main phases of under-thrusting took place along the Cantabrian margin as well as subduction of Iberia under the European plate leading to the formation of the Pyrenean Mountain Belt, an asymmetric double-vergent orogenic wedge, which is more developed on its southern side [*Muñoz*, 1992].

[7] Apatite fission track studies and facies analysis of sedimentary sequences in basins next to the main mountain chains have shown that since the late Eocene to late Oligocene, the Cantabrian Mountains-Pyrenees border was uplifted [*Martín-González et al.*, 2006]. At the same time the asymmetric Spanish Central System was activated, in the beginning along its western sector (Eocene) and finally through the Guadarrama sector during the early Miocene

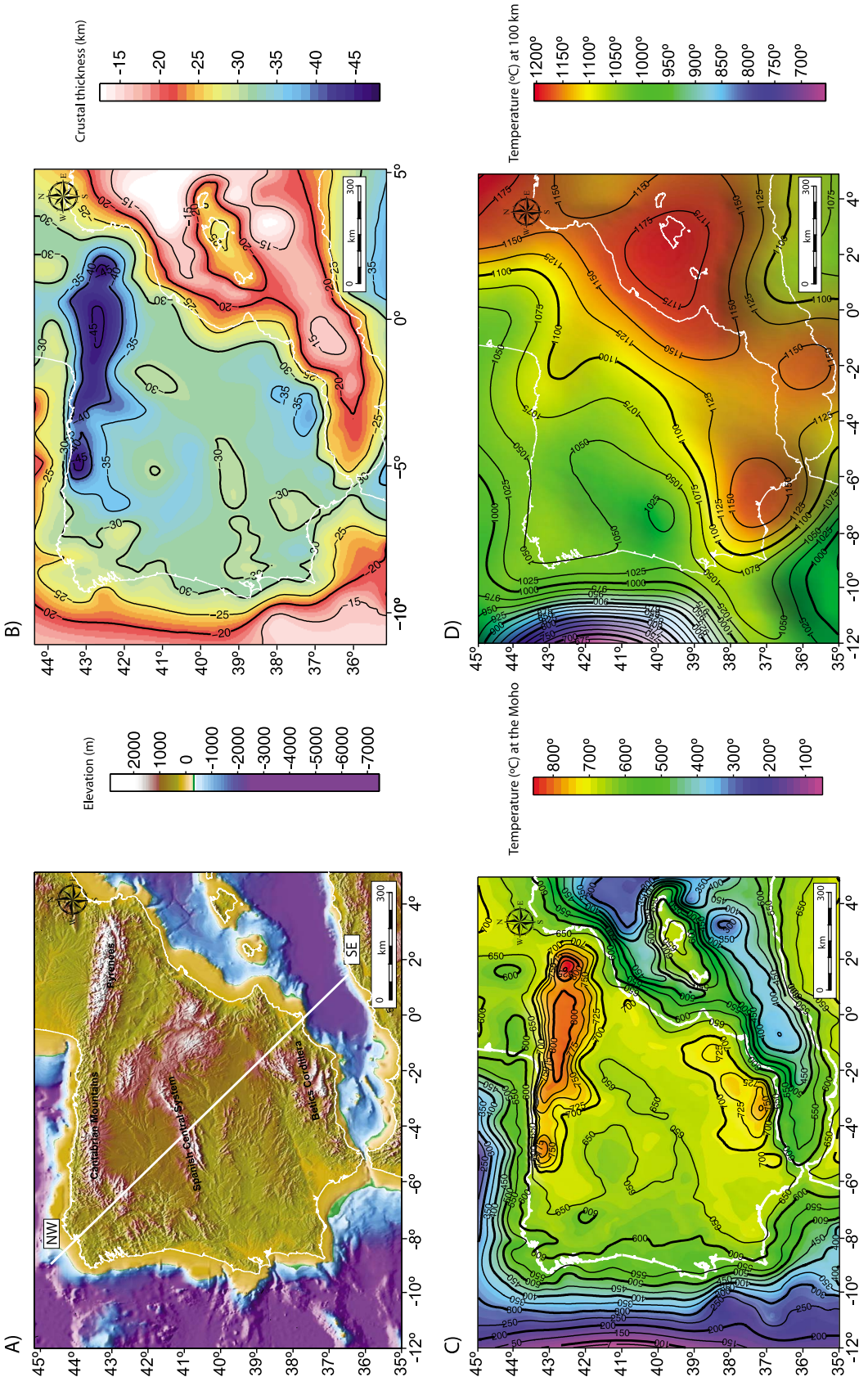

Figure 3

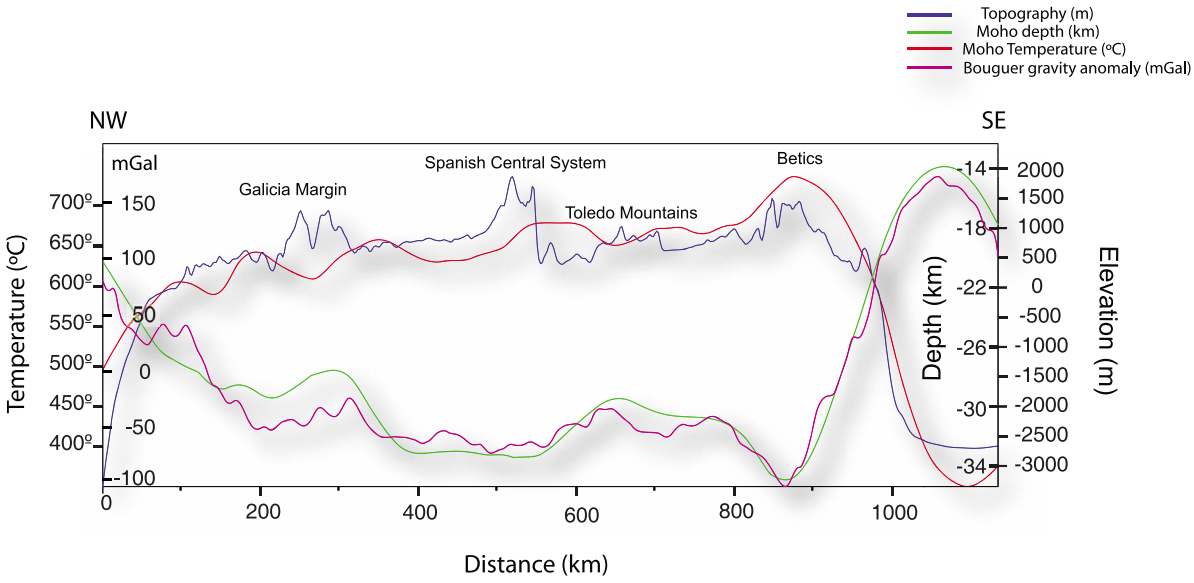

Figure 4. NW-SE Profile through Iberia showing the relationship between surface topography, Bouguer gravity anomaly, crustal thickness, and temperature at the Moho after *Mezcua and Benarroch* [1996]. See Figure 3 for location.

[*De Bruijne and Andriessen*, 2002]. Meanwhile Mesozoic sedimentary basins of the present-day Iberian Chain underwent an oblique inversion from late Eocene to early Miocene [*Del Río et al.*, 2006; *De Vicente et al.*, 2009] which is compatible with the N-S convergence during the Pyrenean Stage.

[8] During the late Oligocene, the opening of the King's Trough in the Atlantic margin together with the opening of the Valencia Trough influenced the orientation of the Sh_{max} trajectories, which turn into E-W orientation in the King's Trough region, NNE orientation at the eastern end of the Pyrenees and NE orientation in the Valencia Trough as constrained by paleostress data [*De Vicente et al.*, 2007] (Figure 2).

[9] From late Oligocene onward Iberia has been part of the Eurasian plate. Kinematic models for present-day plate motions [*Minster and Jordan*, 1978; *Argus et al.*, 1989] and the distribution of earthquakes show that Iberia is actively deforming as part of Eurasia [*Srivastava et al.*, 1990]. The extrusion of the Alboran block towards the southwest was followed by collision of this microterrane during the early Miocene giving rise to the Betics (second stage of Alpine Orogeny). The distributed deformation model proposed by *Vegas et al.* [1990] based on paleomagnetism and plate kinematic models shows how the deformation is dispersed along the Gulf of Cadiz by a mechanism of simple shear. This result suggests strong plate coupling [see also *Ziegler et al.*, 1995, 2002; *Tikoff and Maxson*, 2001] that leads to an efficient stress transmission towards the plate interior. In the area of the Alboran, however, weak coupling between Africa and Iberia has been proposed [*Vegas et al.*, 2008]. Therefore, the reactivation of inherited fault corridors in the western part of the peninsula and actual dominantly shallow seismicity inland is probably triggered by the transfer of the deformation from the recent plate boundary towards the intraplate area (Figure 1b).

[10] It is worth mentioning that preexisting late Variscan faults (mainly strike-slip and normal faults) [*Arthaud and Matte*, 1977] are preferred sites where deformation localized during Alpine contraction. Reactivation of these faults with NE-SW to NW-SE orientation as normal displacement during Mesozoic times led to thick sequences of Triassic to Cretaceous sediments all over the Iberian Chain, followed by an episode of tectonic inversion during most of the Cenozoic [*Guimerà et al.*, 1996] (Figure 1a). In central Spain, these fault system were also reactivated leading to the tectonic inversion of subsiding areas, giving rise to a series of mountain ranges (clear examples are the Spanish Central System and Toledo Mountains, *De Vicente and Vegas*, 2009). The localization of deformation due to the presence of preexisting basement faults and their control during subsequent tectonic inversion have also been highlighted in other areas of intraplate deformation like the Colombian Cordillera [*Cortés et al.*, 2006], the Atlas system in northern Africa [*Teixell et al.*, 2003], or the U.S. Rocky Mountains [*Tikoff and Maxson*, 2001].

3. The Iberian Lithosphere

[11] In recent years, studies addressing the Alpine tectonics in Iberia have demonstrated the contribution of in-

Figure 3. (a) Topographic map of Iberia. The NW-SE trending line gives the location of the cross section displayed in Figure 4. (b) Crustal thickness map (km) (data from *Tesauro et al.* [2008]). (c) Temperature (°C) at the Moho and (d) temperature variation at 100 km depth. (data from *Tesauro et al.* [2010]).

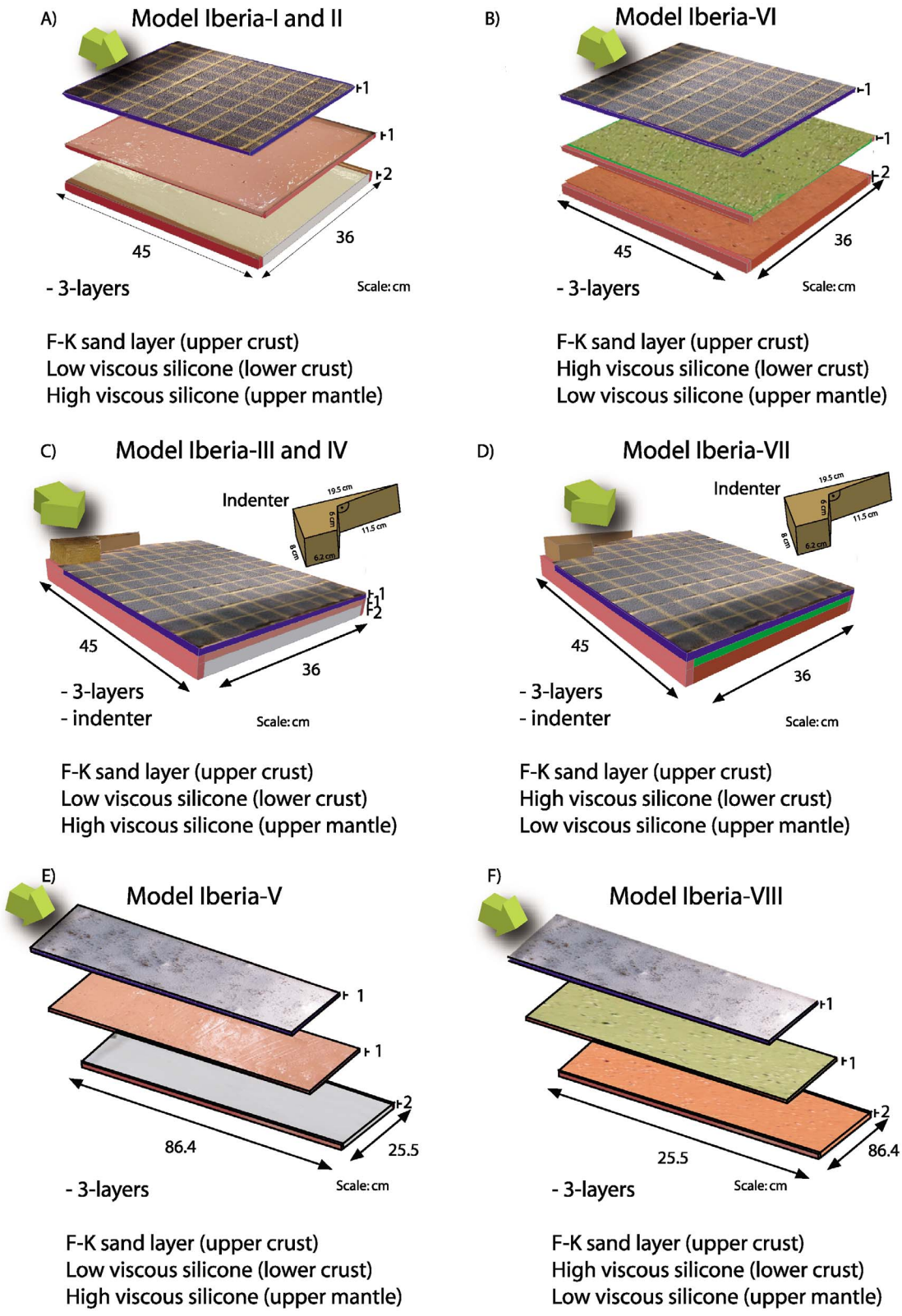

Figure 5. Model setup for experiments for normal lithosphere (a) Iberia I and III, (convergence rate equivalent to 0.5 cm h^{-1}). (b) Iberia II and IV (convergence rate equivalent to 1 cm h^{-1}). See Table 1 for material properties and natural equivalent. Grid spacing is 4 cm. (c) Iberia V (convergence rate 0.5 cm h^{-1}) and (d) inverted lithosphere (convergence rate 0.5 cm h^{-1}).

Table 1. Physical Properties and Layer Thicknesses of the Lithosphere and Experimental Materials

Layer	Density ρ (kg m^{-3})	Viscosity η (Pa s)	Layer Thickness h (m)	Coefficient of Friction μ	Velocity v[a] (m s^{-1}) Experiments I and III	Velocity v[a] (m s^{-1}) Experiments II, IV, and V	Rm[b]
Iberia I, II, III, IV, and V							
Upper crust nature	2670	–	1.50E+04	0.4	7.00E−03	1.40E−02	–
Upper crust model	1330	–	1.00E−02	35 Pa (cohesion)	5.00E−03	1.00E−02	–
Lower crust nature	2900	1.00E+21	1.50E+04	–	7.00E−03	1.40E−02	28.83
Lower crust model	1486	2.08E+04	1.00E−02	–	5.00E−03	1.00E−02	21.86
Upper lithosphere mantle nature	3400	4.00E+21	3.00E+04	–	7.00E−03	1.40E−02	33.80
Upper lithosphere mantle model	1606	1.87E+05	2.00E−02	–	5.00E−03	1.00E−02	36.86

Layer	Density ρ (kg m^{-3})	Viscosity η (Pa s)	Layer Thickness h (m)	Coefficient of Friction μ	Velocity v[a] (m s^{-1})	Rm[b]
Iberia VI, VII, and VIII						
Upper crust nature	2670	–	1.50E+04	0.4	7.00E−03	–
Upper crust model	1330	–	1.00E−02	35 Pa (cohesion)	5.00E−03	–
Lower crust nature	2920	1.00E+22	1.50E+04	–	7.00E−03	29.03
Lower crust model	1511	1.87E+05	1.00E−02	–	5.00E−03	22.23
Upper lithosphere mantle nature	3350	1.00E+21	3.00E+04	–	7.00E−03	33.31
Upper lithosphere mantle model	1590	2.30E+04	2.00E−02	–	5.00E−03	36.49

[a]Velocity values correspond with convergence rates from models and nature.
[b]Values of Ramberg number (Rm) of model and natural analogue.

traplate deformation to creation and distribution of mountain ranges. In order to better understand the recent and ongoing lithospheric processes in Iberia, integration of seismic and gravity data, analysis of topography and stresses is vital [*Banda et al.*, 1996, 1983; *Choukroune and ECORS Team*, 1989; *Choukroune et al.*, 1990; *Roure et al.*, 1989; *Simancas and Carbonell*, 2003; *Carbonell et al.*, 2007; *Suriñach and Vegas*, 1988; *Roca et al.*, 2008].

3.1. Crustal Structure and Topography

[12] The most striking feature observed from satellite images and topographic maps is the regular distribution of E-W to NE-SW trending mountain ranges and Tertiary basins in Iberia and their relatively high mean altitude of more than 600 m, which is one of the highest topographic averages in Europe.

[13] The comparison between the spectrum obtained from the Bouguer gravity anomalies and the signal provided by the undulations produced by the topography (Figures 3a and 3b) show different wavelengths, the smaller ones around 50–80 km and the largest ones (250–500 km) related to crustal and mantle deformation, respectively [*Cloetingh et al.*, 2002; *Muñoz-Martin et al.*, 2011]. Recently, *Tesauro et al.* [2007, 2008] provided an integrated study of the lithospheric properties of the European lithosphere based on seismic tomography, seismic reflection and refraction, and receiver function data. Their results show large crustal thickness variations in Iberia with maximum values in the Pyrenees-Cantabrian Mountains, Central Iberia and the Betic Cordillera (50, 35, and 40 km respectively), which are also portrayed by distinct negative gravity anomalies (Figure 4).

[14] Reflection and refraction profiles along the Cantabrian Mountains [*Gallastegui et al.*, 1997] and Sierra Morena [*Simancas and Carbonell*, 2003] recognize the presence of a reflective middle crust which appears not to be continuous for the whole peninsula, but restricted. The above named regions contrast with the less negative Bouguer anomalies of the main basins, which are correlated with a relative shallow position of the Moho (circa 29–30 km). In addition, in the north western most corner of Galicia, the crust is thinner as a result of the opening of the Atlantic Ocean and passive margin formation.

3.2. Thermal Structure and Rheology

[15] The thermal structure of the Iberian lithosphere (Figures 3c and 3d) has been linked to the combined effect of the latest tectonic events and inherited crustal-mantle heterogeneities. As a result, the thermal state of the lithosphere has been modified leading to large differences between thermal conditions close to the surface and in great depth. These differences are the final expression of the Mesozoic Rifting and later Alpine compression during the Tertiary times.

[16] Recent heat flow data compiled by *Fernández and Marzán* [1998] show high values along the eastern part of Iberia, close to 100 mW m^{-2}, and in the south western area of the Portuguese Algarve with an average of 60–80 mW m^{-2}. Additionally, *Tejero and Ruiz* [2002] obtained results between 60 and 70 mW m^{-2} for the main plate interior, showing that the mantle heat flow increases with diminishing surface heat flow. Based on these results, the authors calculated strength profiles from the Iberian lithosphere that predict a brittle mantle below the Duero and Tagus Basins and a relatively weak mantle under the Spanish Central System (Figures 6a–6c), which might be related to the thickening of the lower crust as suggested from seismic refraction profiles by *Suriñach and Vegas* [1988].

[17] In addition, Moho temperatures calculated by *Tesauro et al.* [2007] show maximum values under the Pyrenees and the Betics, which are related to the root of either orogen. Predicted lateral temperature variations at

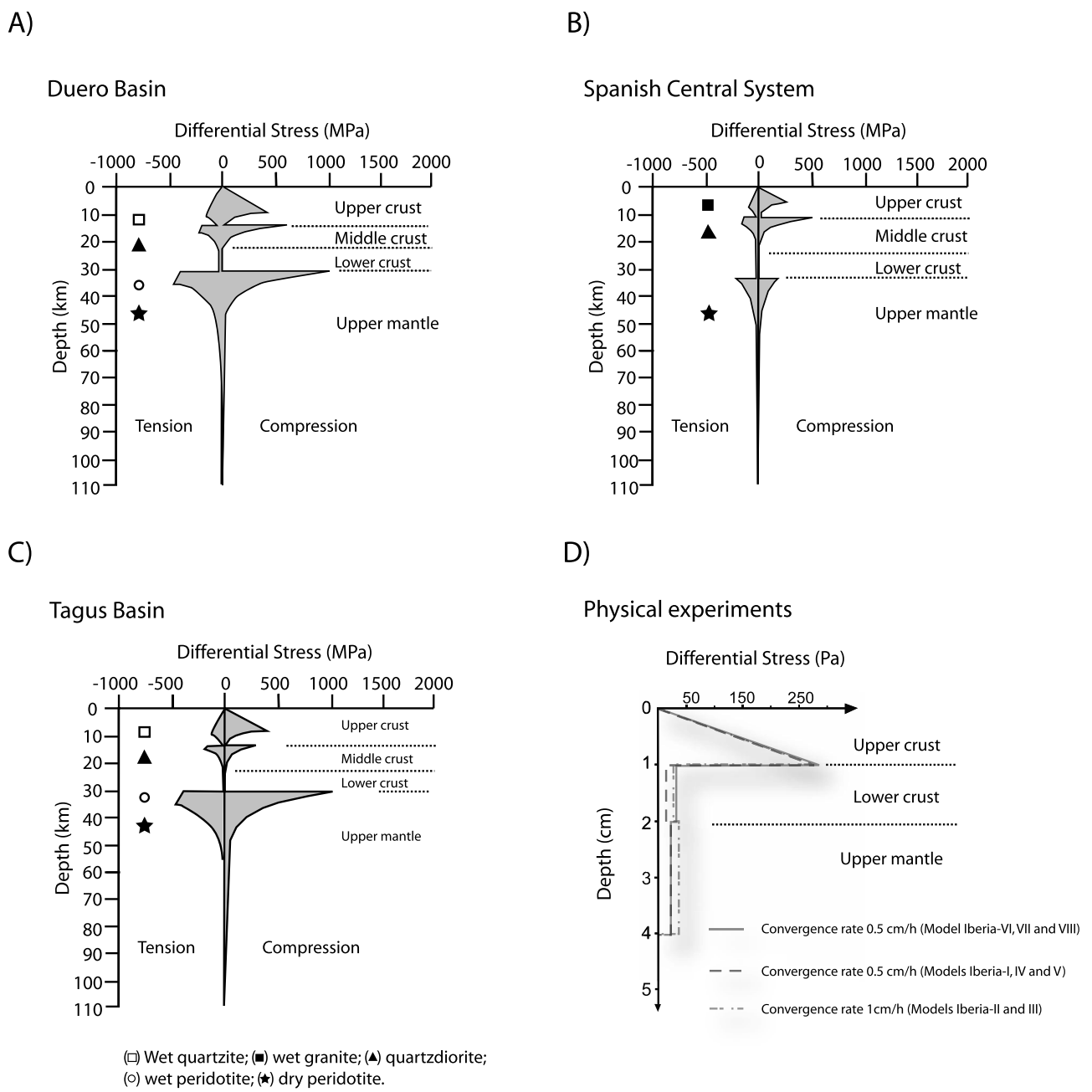

Figure 6. Lithosphere strength profiles from (a) the Duero Basin, (b) the Spanish Central System, and (c) the Tagus Basin at 60, 70, and 65 mW m^{-2}, respectively, calculated by *Tejero and Ruiz* [2002]. (d) Strength profiles before deformation from inverted lithosphere (Iberia VI) experiment and (e) normal lithosphere at a convergence rate of 0.5 cm h^{-1} (Iberia I, IV, and V) and (f) normal lithosphere at 1 cm h^{-1} (Iberia II and III).

Figure 7. (a) Structural interpretation of top view images and digital elevation model (DEM) from model Iberia I for three incremental stages of deformation. See text for further explanation. Arrows show the direction of convergence. (b) Finite state of the three-dimensional (3D) structure of model Iberia I. The ductile lithosphere is slightly folded (lower crust and upper mantle) whereas the upper crust is thrusted by pop-ups and single thrusts. Arrows show the direction of shortening. The amount of bulk shortening in Figures 7a and 7b has been scaled to nature. Numbers indicate temporal evolution of structures. Ellipsoids represents intramountain basin and stars represent intermountain basins without taking into account temporal evolution.

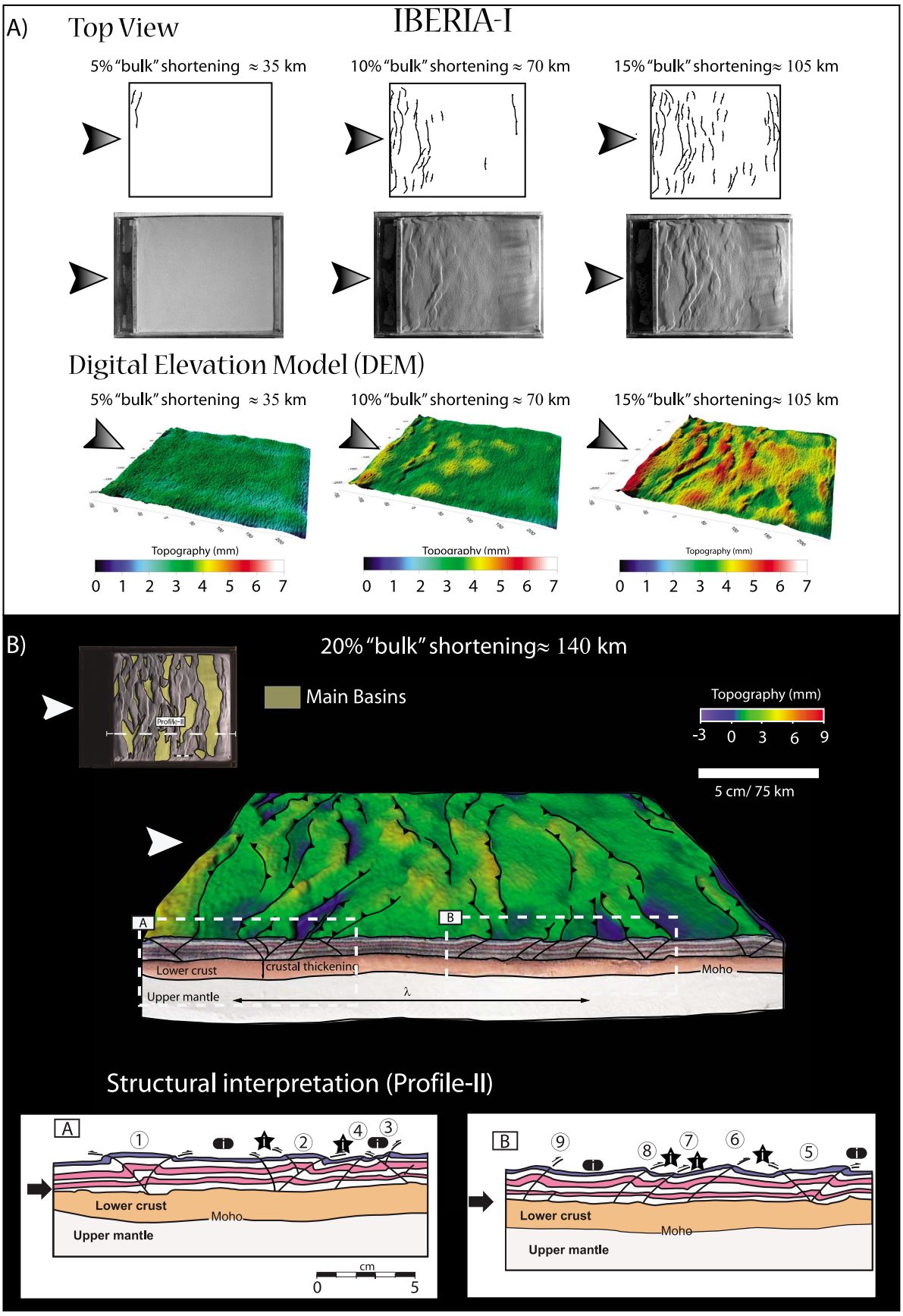

Figure 7

100 km depth along a NE-SW zone in southeastern Iberia could be the result of different processes occurring since the early Miocene, such as the opening of the Valencia Trough, extension in the Catalan Coastal Ranges, and overthrusting of the Alboran block.

[18] All the above mentioned data were used by *Van Wees and Cloetingh* [1996] and *Ruiz et al.* [2006] to estimate the elastic properties of the Iberian lithosphere. The seismogenic thickness (*Ts*) is close to 10–17 km (see inset in Figure 1b) while the value obtained for the effective elastic thickness (*Te*) reaches 24 km which is compatible with the seismic activity in the intraplate domain restricted to the upper crust [*Martín-Velázquez et al.*, 2009]. The lower crust and upper mantle of Iberia are essentially devoid of seismicity.

[19] Based on these data, the Iberian lithosphere is probably composed of a brittle upper crust, a ductile weak lower crust, and a relatively strong mantle.

4. Experimental Setup

4.1. Geometry, Rheology, and Scaling

[20] The experiments were performed in a rectangular Plexiglas box with transparent vertical sidewalls. One wall was mobile and acted as an indenter. The moving wall was connected to a low frequency electric engine through a screw jack. Velocities adopted for this study are 0.5 and 1 cm h^{-1}.

[21] The three-layer models (Figure 5) consist of ductile, slightly non-Newtonian silicone (PDMS or Rodorsil Gomme mixtures) layers representing the upper mantle and lower crust, respectively. A K-feldspar sand layer represents the brittle upper crust. These layers, which are characterized by the properties listed in Table 1 rest on an asthenospheric material made of a mixture of polytungstene and glycerol to ensure isostatic equilibrium. The experiments have been performed under normal gravity conditions. A laser scan has been used to obtain the digital elevation model (DEM) combined with top view pictures taken with a digital camera at constant time rate during evolution of the model.

[22] Main variables investigated in this study comprise convergence rate changes and hence the degree of crust-mantle decoupling, the strength of the lower crust and upper mantle, and the geometry and length of the experiments. The latter ensures that the resulting wavelengths of deformation were not biased by the model dimensions (see Tables 1 and 2 and Figure 3).

[23] Following *Ramberg* [1967] and *Weijermars and Schmeling* [1986], scaling of the experiments was based on geometric, kinematic and dynamic similarity between model and natural prototype, Iberia. Scaling parameters are displayed in Table 1 and are constrained by geophysical and geological data from Iberia (see section 3). Dynamic similarity obtained through dimensional analysis is based on the Ramberg Number (R_m) [*Weijermars and Schmeling*, 1986; *Sokoutis et al.*, 2000] and the Smoluchowsky Number (*Sm*) [*Ramberg*, 1981; *Mulugeta*, 1988] for the viscous and brittle behaviors, respectively:

$$R_m = \rho g l^2 / \eta V, \tag{1}$$

$$S_m = \rho_b g h_b / c + \mu \rho_b g h_b, \tag{2}$$

where ρ and ρ_b are the density of the ductile and brittle materials respectively, g is the gravity acceleration, l and h_b the thicknesses of the ductile and brittle layers, c the cohesion, η the viscosity, V the velocity and μ the friction coefficient.

[24] For the brittle part of the lithosphere under compression, differential stresses were calculated following the equation [*Anderson*, 1951; *Weijermars*, 1985]:

$$\tau = 2[c_o \mu \rho z(1-\lambda)] / \left(\mu^2 + 1\right)^1 / 2 - \mu, \tag{3}$$

where τ is the differential stress, C_o is cohesion, μ is the coefficient of friction, ρ is the density, z is the layer thickness, and λ is the pore pressure (assumed to be insignificant in the models).

[25] For the ductile layers, the differential stress is resolved by the equation:

$$\tau = \eta \nu, \tag{4}$$

where τ is the differential stress, η refers to viscosity, and ν refers to convergence rate, respectively (Figure 6d).

4.2. Simplifications and General Assumptions

[26] In this study we assume an initially homogeneous lithosphere, which is devoid of lateral changes in composition, temperature and/or rheology or inherited structures. It has been shown by *Willingshofer et al.* [2005] and *Willingshofer and Sokoutis* [2009] that weak zones in the lithosphere are important for governing wavelength and amplitude of deformation, but do not necessarily influence its style or dominant deformation mechanism, which has been inferred to be related to the presence of decoupling zones [*Willingshofer and Sokoutis*, 2009; *Luth et al.*, 2009]. We are fully aware that preexisting structures are important for the localization of Alpine contractional deformation, the topic of an upcoming manuscript.

[27] Erosion and sedimentation are controlled by tectonic and climatic processes. The models presented here assume the onset of mountain building during the Africa-Iberia convergence when morphoclimatic processes would de-

Figure 8. (a) Structural interpretation of top view images and DEM from model Iberia II. See text for further explanation. Arrows show the direction of convergence. (b) Cross section along profile II (see inset) showing more complex structures than previous model developed in the brittle part of the crust. In inset boxes a and b from profile, arrows show the direction of shortening and numbers refer to the temporal evolution of structures. Ellipsoids represents intramountain basin and stars intermountain basins without taking into account temporal evolution.

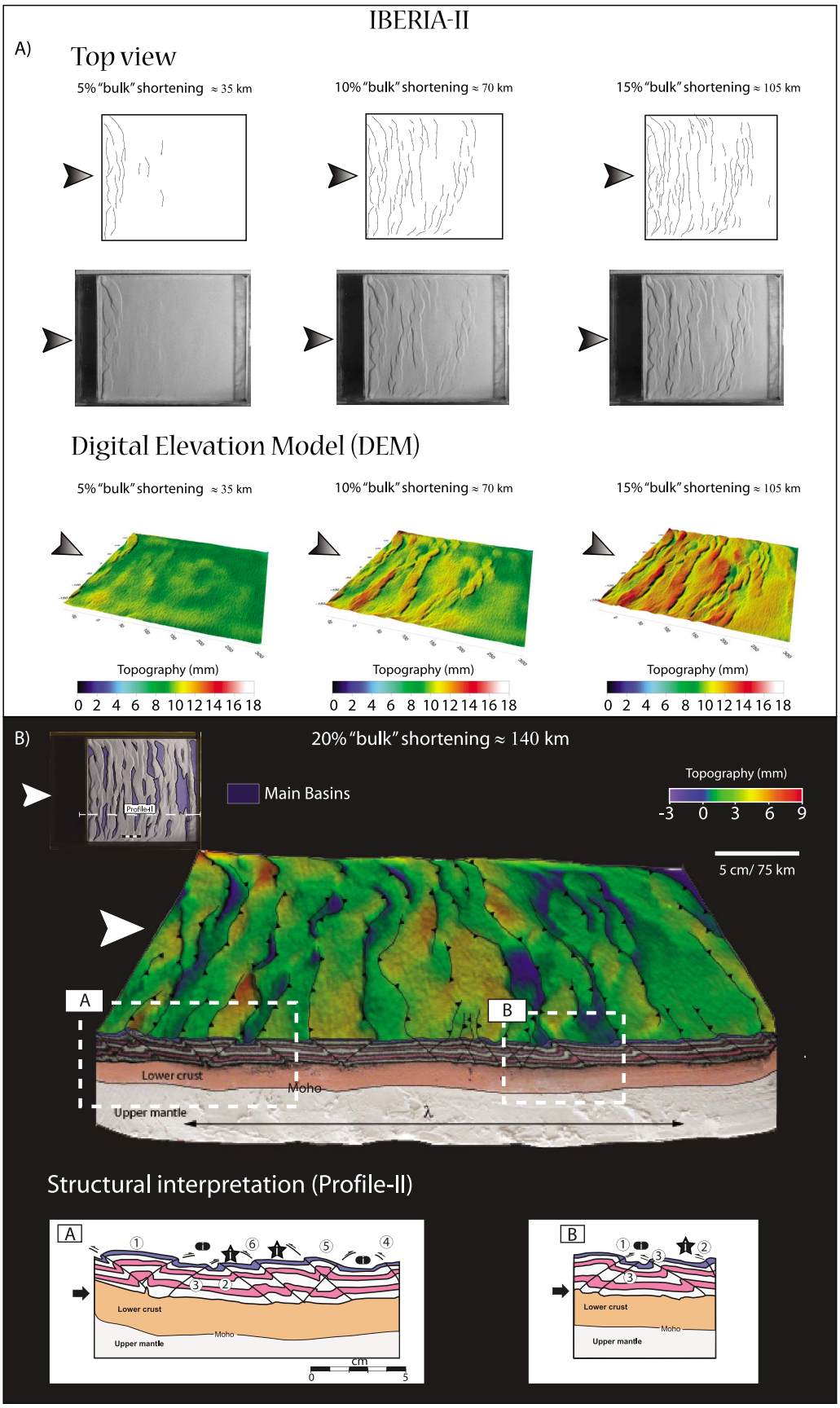

Figure 8

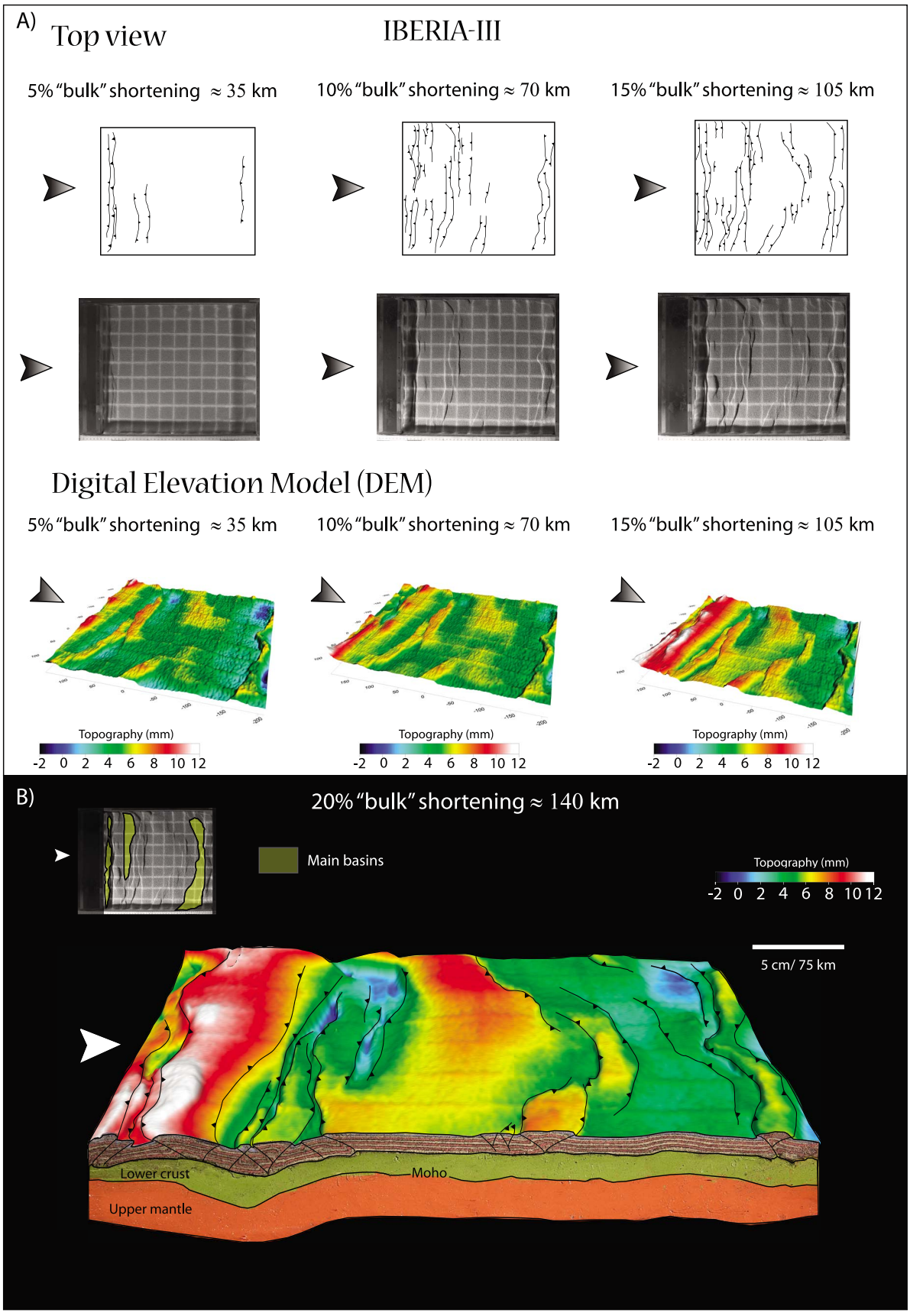

Figure 9

velop slowly across the entire peninsula without significant changes in basin configuration.

[28] The opening of the King's Trough in the north western corner of the Atlantic margin of Iberia (see Figure 2) led to the establishment of constrictional deformation conditions within the Iberian Plate during the early Tertiary, as well as the transfer of the stresses along a series of fault corridors in the western part of the microplate during the Paleogene. In experiments Iberia III and Iberia IV we implemented a rigid indenter aiming at investigating the influence of an oblique (NW-SE oriented) stress component on the deformation of the northwestern part of Iberia.

[29] The analogue experiments were shortened by 20% at a constant rate, representing the bulk shortening affecting central Iberia during the Pyrenean stage of the Alpine Orogeny [*De Vicente et al.*, 1996]. The collision rate in Iberia, however, fluctuated through time from periods of high to low convergence from Late Cretaceous to middle Miocene.

5. Modeling Results

5.1. Crust-Mantle Coupling

[30] Variations of convergence rates are used to investigate the influence of crust-mantle coupling on the deformation of the model lithosphere.

5.1.1. Model Iberia I: Weak Crust-Mantle Coupling

[31] Experiment Iberia I serves as a reference for the other models. After 5% of bulk shortening, a pop-up structure developed close to the moving wall. With increasing shortening, these thrusts propagate laterally while newly formed thrusts do not develop immediately in front of the older ones as often observed in fold and thrust belts (imbricated thrusts), but at a distance, which is larger than the width of the first pop-ups (Figure 7a). At 15% of shortening, deformation reached the opposite wall. Small curved forethrusts and backthrusts develop and the distance between clusters of thrusts is reduced (cross section, Figure 7b). At the end of the experiment, deformation was distributed over the entire length of the model as new small pop-ups developed in between the former structures and small basins formed in between relatively wide pop-ups and thrusts, suggesting that shortening was taken up by many structures with limited amount of displacement.

[32] Digital elevation models (Figure 7a, lower image) show that the relief is structurally controlled and hence evolves through time as thrusts and pop-ups propagate. By the end of the experiment the finite topography reflects general uplift with narrow intervening depressions.

[33] In cross section the geometry of the brittle crust is controlled by thrusts, pop-ups, and pop-downs (e.g., between thrusts 3 and 4, see Figure 7b, inset a). Slight thickness variations in the ductile crust correlate with the location of the pop-ups and thrusts in the upper crust such that thickening occurred at the locations of the upper crust structures, which also coincide with the locations of synforms of gentle, long wavelength folds of the upper mantle layer.

5.1.2. Model Iberia II: Strong Crust-Mantle Coupling

[34] Deformation in experiment Iberia II is concentrated close to the moving wall during the first 8% of bulk shortening. Different from Iberia I, thrusts and pop-ups occupied most of the model space already after 10% of bulk shortening with the distant thrusts being arranged in an en echelon fashion (Figure 8a). Small intervening basins dominantly have elongate shapes. In the later stage the deformation appears more distributed and there is no relative advance towards the static wall. New small thrusts appear in areas that were not deformed before. After 20% of bulk shortening numerous thrusts cut most of the model surface separating depressions between them (Figure 8).

[35] Unlike the previous model, general uplift occurs since the beginning of shortening; at 15% of bulk shortening highest elevations are reached. However elevations seem to be aerially distributed at later stages of deformation through the entire model (compare DEM models from Figures 7a and 8a, lower images in both).

[36] Faulting in model Iberia II is more distributed along the surface. Most of the brittle structures appear to have nucleated on the ductile lower crust which accommodates deformation by flowing over the mantle, causing vertical uplift. The spacing of thrusting is shorter compared to experiment Iberia I.

[37] The upper crustal architecture as displayed in Figure 8b is dominantly characterized by pop-up (inset a) and pop-down (inset b) structures and imbricate thrusts mainly occur between the main pop-ups. During an episode of forward thrusting (up to 10% of bulk shortening (BS)) intermountain basins developed, which have subsequently been deformed by back thrusting. The viscous upper mantle displays gentle long wavelength low amplitude folding and the geometry of the ductile lower crust is governed by the upper crust and upper mantle geometries, respectively.

5.2. Rheology of the Lower Crust and Upper Mantle

[38] In experiment Iberia III the viscous lower crust is stronger than the upper mantle resembling a crème brûlée-type rheology of the lithosphere [e.g., *Jackson*, 2002]. Soon after the onset of shortening thrusts appear close to the moving wall (Figure 9a). After 10% of deformation, thrusting jumped to the inner part of the model. The first intermountain basins (referred here as foreland basin between two mountain chains) developed at this stage (DEM images, Figure 9a). Surface uplift is concentrated close to the moving wall, where it can be linked to the development of thrusts and pop-ups, as well as in the middle part of the model, where controlling structures are largely missing at the surface. With the advance of shortening, the inner part of

Figure 9. (a) Structural interpretation of top view images and DEM from model Iberia III (weak mantle under convergence rate of 0.5 cm h^{-1}). See text for further explanation. Arrows show the direction of convergence. (b) 3D model after 20% of bulk shortening shows two broad antiforms (white arrow indicates direction of shortening).

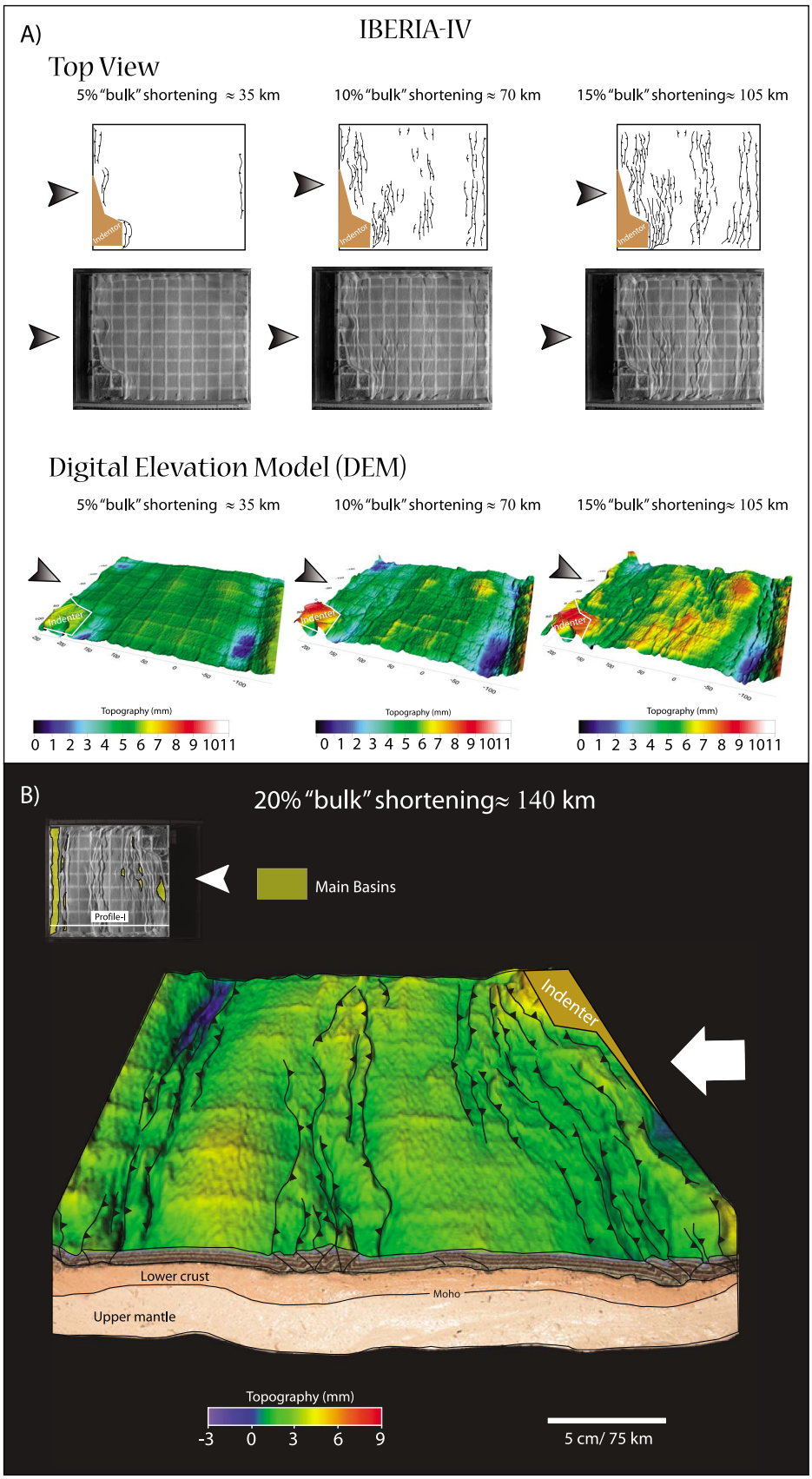

Figure 10

the model started to deform by pop-ups, which are arranged in an en echelon fashion. At the same time earlier formed basins became shortened and partly consumed under the mountain ranges pop-ups. New basins appear in the forefront of the thrust (Figure 9b).

[39] The cross section (Figure 9b) resembles the geometry of a folded lithosphere with well developed synforms and antiforms. The amplitude of folding is a function of the distance to the advancing wall. Furthermore, the cross section reveals that the broad, uplifted zone in the centre of the model is controlled by folding of the viscous layers rather than upper crustal basins.

5.3. Influence of an Indenter

5.3.1. Model Iberia IV

[40] This experiment aimed at testing the effect of constriction produced by the opening of the King's Trough in the north western part of the Iberian Atlantic platform [see *Cann and Funnell*, 1967; *De Vicente and Vegas*, 2009] and its effects on the pattern of intraplate deformation in Iberia. Accordingly, we use an indenter to observe if there is effective deformation transfer from the moving wall towards the inner part of the model. In contrast to the previous models, we observed deformation being concentrated within zones of finite width (Figure 10), which are separated from nearly undeformed parts of the model. This general pattern of deformation was already established after 10% BS. Thereafter, shortening led to the lateral propagation of thrusts and to a minor extent to the generation of new structures. Strongly deformed regions dominantly correlate with topographic lows suggesting that deformation of the upper crust is incapable of explaining the monitored topography.

[41] The wavelength of the deformation is highlighted by the indenter geometry as the same amount of shortening is applied over different initial lengths of the model. Topographic uplift is clearly defined along two central antiforms followed by two broad basins at both sides (blue areas in the DEM images at 20% BS; Figure 10a, lower panel). Cross sections show that the upper mantle and lower crust are folded and thickened. The lower crust is thickened in areas where the Moho is depressed and main mountain ranges are localized. A stage of basin development is rapidly followed by uplift influenced by the down warping of viscous layers and in some cases by crustal structures (i.e., blind thrust).

5.3.2. Model Iberia V

[42] The setup of experiment Iberia V is similar to the previous except that the convergence rate has been doubled to 1cm h^{-1} (~14 mm yr^{-1}). In the first stages of shortening, deformation is localized close to the moving wall and ahead of the indenter (Figure 11a). Close to the moving wall, brittle structures develop oblique to the shortening direction as a result of indenter geometry. Thrusting advanced forward leading to overall deformation of the model surface. Similar to experiment Iberia III, localization of structures occurred in regularly spaced zones, which are separated by largely undeformed regions.

[43] The cross section portrays large-scale folding of the model lithosphere (Figure 11b), which seems to control the distribution of brittle structures such that they mainly coincide with the synforms of the folds. Compared to model Iberia IV, the amplitude of the folds is higher but thickness variations of the ductile layers are subdued, suggesting that more shortening was taken up by folding than concurrent thickening of the layers.

5.3.3. Model Iberia VI

[44] Experiment Iberia VI is characterized by a strong lower crust and a weak upper mantle and the presence of an indenter (see Figure 5 for details). The first thrusts appear close to the advancing wall as well as the rigid wall (Figure 12a). Further shortening led to the development of the first pop-up in the central part of the model at about 10% BS. Similar to experiment Iberia III shortening has been taken up by fewer structures, which are regularly spaced. Structures in the brittle crust are pop-ups, for example, in the centre of the model or pop-downs, that is, close to the moving wall (Figure 12c). The location of these structures coincides with the position of synforms of the folded ductile layers. Two big antiforms without internal deformation, which developed between narrow synforms, correspond to regions of high elevation and a shallow Moho. In places where displacement along a single structure was significant (e.g., the backthrust confining the pop-down close to the advancing wall), the ductile crust and upper mantle are advected upward leading to pronounced lateral thickness variations in the weak upper mantle.

5.4. Role of Model Size

[45] Model Iberia VII, which is distinctly longer than the previous ones, serves to ensure that the results described above are of significance and not influenced by the length of the box.

[46] Buckling of the lithosphere became evident during the first phase of shortening. Three pronounced uplifted regions developed close to the advancing wall prior to the formation of thrusts (see 5% BS DEM image in Figure 13a). Wavelength and amplitude of folds was similar to the models performed in a shorter box suggesting their independence to the chosen model length. Further shortening localized uplift along the previous structures giving rise to

Figure 10. (a) Structural interpretation of top view images and DEM from model Iberia IV. See text for further explanation. Arrows show the direction of convergence. (b) 3D image representing model Iberia III from profile I (see inset). Ductile layers are folded and heterogeneously thickened along the main synclines where mountain ranges developed. The model shows two wide, uplifted basins developed between thrust systems. Some blind thrusts within the basins produce uplift in later stages of deformation. This process may lead to high altitudes in areas like the Duero Basin in Iberia. Numbers refer to temporal evolution of thrusting. Ellipsoids represents intramountain basin and stars intermountain basins without taking into account temporal evolution.

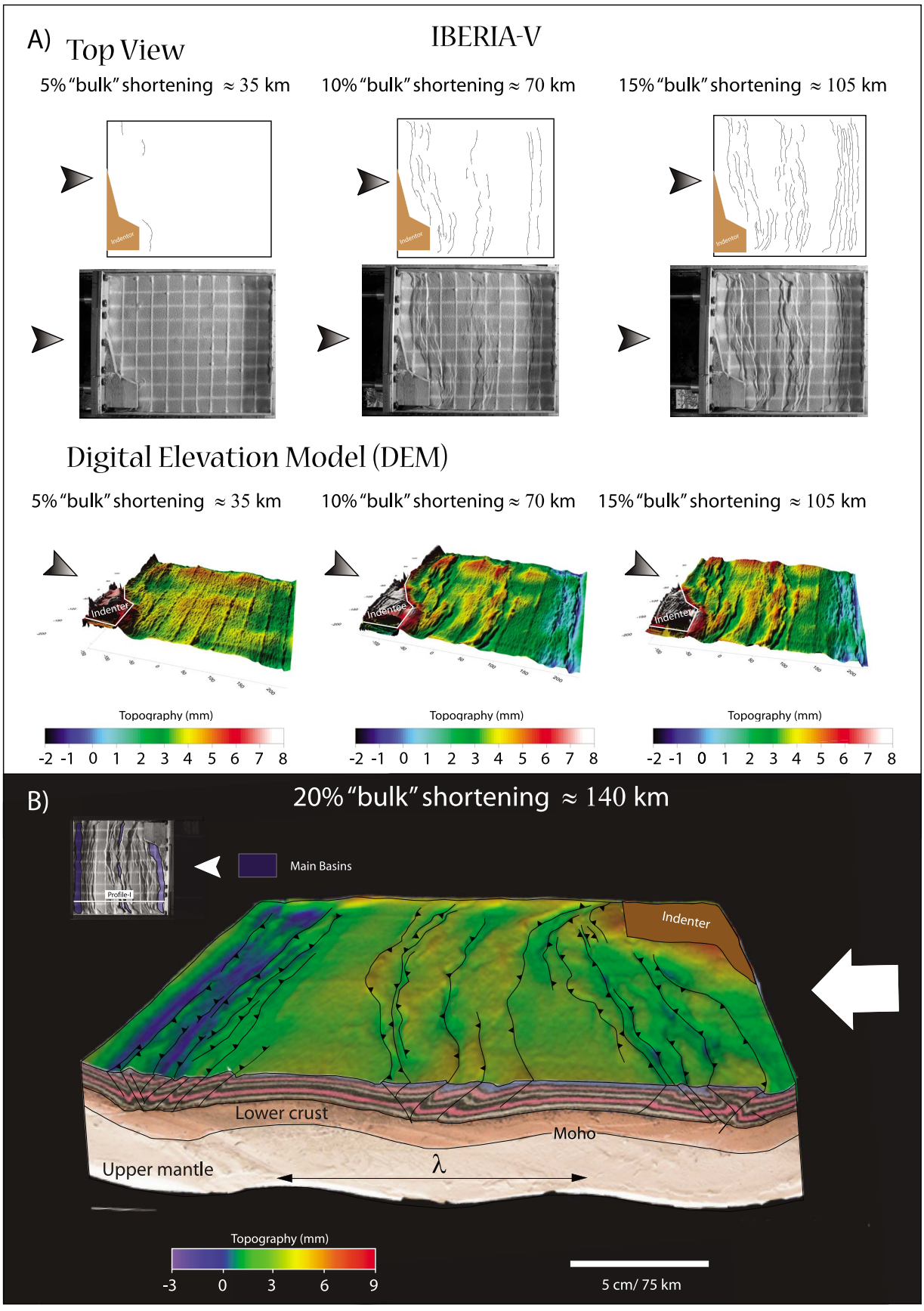

Figure 11

well-developed antiforms. Mountain ranges are the result of single thrusts and pop-ups which rolled over from elevated areas to the position of lithosphere synforms probably pushed by the flow of the ductile crust. However, the initial position of basins remains unchanged.

[47] The final stage of deformation shows an important reduction of spacing between pop-ups close to the moving wall (Figure 13b, structural interpretation in inset a). However towards the central part of the model, wider pop-ups are formed (inset b in Figure 13b). Differences in pop-up spacing support the idea of strain localization along the margin which is also apparent from the thickening of the lower crust and geometry of folding surfaces.

6. Summary of Modeling Results

[48] Our experiments show that the development of regularly spaced mountain belts may be the result of folding. In general, the spacing of thrust systems and basin shapes are linked to fold wavelength, which has been investigated through changing the convergence rates adopted for models. Higher convergence rate induces distribution of deformation along the model and supports major crustal-mantle coupling unlike the effects of low convergence rate.

[49] The presence of an indenter leads to obliquity of surface structures and localizes deformation. The change on model geometry influences the position of elevated areas close to the indenter.

[50] Finally, the long-dimension model successfully explains the topography observed as a result of folding without being influenced by box length. Therefore, the evolution and position of topography is linked to wavelength and amplitude of folding of the ductile layers.

[51] Our results show strong variations on style and spacing of thrusting regarding rheological variations of lithospheric layers. These differences also influence the position and evolution of developed basins. Models with a weak lower crust and strong mantle show relatively symmetric thrusting and spacing influenced by convergence rate. However, models performed with a strong lower crust and weak mantle show asymmetry in modes of deformation. Thickening of the lower crust is evidenced on the topographic surface by close distribution of thrusts in contrast with the lithosphere with strong lower crust, where significant flow occurred in the mantle.

7. Discussion of Modeling Results

7.1. Relationship of Folding and Faulting

[52] The results of the analogue models suggest that the first response to shortening of a rheologically stratified lithosphere with uniform mechanical properties of each layer is buckling. Thrusting is developed at the very beginning of deformation along the inflexion points of the antiforms [*Davy and Cobbold*, 1991; *Martinod and Davy*, 1994]. As the buckling instability amplifies the formation of newly formed structures, such as pop-ups and pop-downs, predominantly occurs at the sides of the synforms, whereas little deformation is observable at the position of the antiforms. On the other hand, folding and faulting could happen simultaneously, and folding may be accommodated by brittle faults as proposed by *Cloetingh et al.* [1999] and *Gerbault et al.* [1999]. Our models show active buckling for the decoupled upper crust and mantle.

[53] In the beginning of deformation, faulting in the upper crust produced by weakening of the system increases the strain rate along a vertical lithosphere segment. The strain distributed vertically towards the mantle led to thickening of the ductile crust. These results are in agreement with numerical modeling performed by *Jarosinski et al.* [2011], where the highest strain rates are localized along the lithosphere synclines.

7.2. Moho and Surface Topography

[54] We have constructed Moho maps to infer the patterns of Moho topography produced by folding of the lithosphere. Figure 14 shows the total crustal thickness of the model Iberia V scaled to nature (see Table 1 for nature and model scaling thicknesses). Abnormally shallow Moho close to the moving wall reflects boundary effects and shall not be discussed here. According to the map in Figure 14, thinning of the crust occurred in regions coinciding with antiforms of the mantle waves, suggesting that flow of the lower crust took place leading to thickening in the synforms and thinning in the antiforms. The deepest part is localized near the indenter and is oblique to the main shortening direction. This is related to the effect produced by the constraining geometry. In addition, topography shown in Figure 11 is located in those areas where the Moho reaches deepest depths. Furthermore, the highest values of elevation are localized close to the moving wall and indenter. However, the amplitude of the synforms seems to modify the mountain range elevation.

[55] The above mentioned results, point out the presence of two different wavelengths affecting the topography and surface of the Moho. Consequently, the topography wavelength is smaller than the mantle folds (represented by ups and downs on the surface of the Moho in Figure 14).

[56] Increasing the shortening velocity enhances the coupling between the lithosphere layers amplifying the wavelengths of the folding (compare Figures 7, 8, 10, and 11). Long distance between thrusts during the early stages of the model deformation suggests that their spacing is controlled by folding of the mantle lithosphere, whereas modification of the folding wavelength is interpreted to reflect deformation of the lower crust.

[57] Numerical models carried out by *Burov et al.* [1993], show the strong dependence of fold wavelength and the

Figure 11. (a) Structural interpretation of top view images and DEM from model Iberia V. See text for further explanation. Arrows show the direction of convergence. (b) Cross section along profile I (see inset). Arrows show the direction of convergence. Ductile layers are folded. The lower crust presents thickening below the synclines where main mountain ranges are localized. The basins are uplifted and appear on top of the lithosphere anticlines.

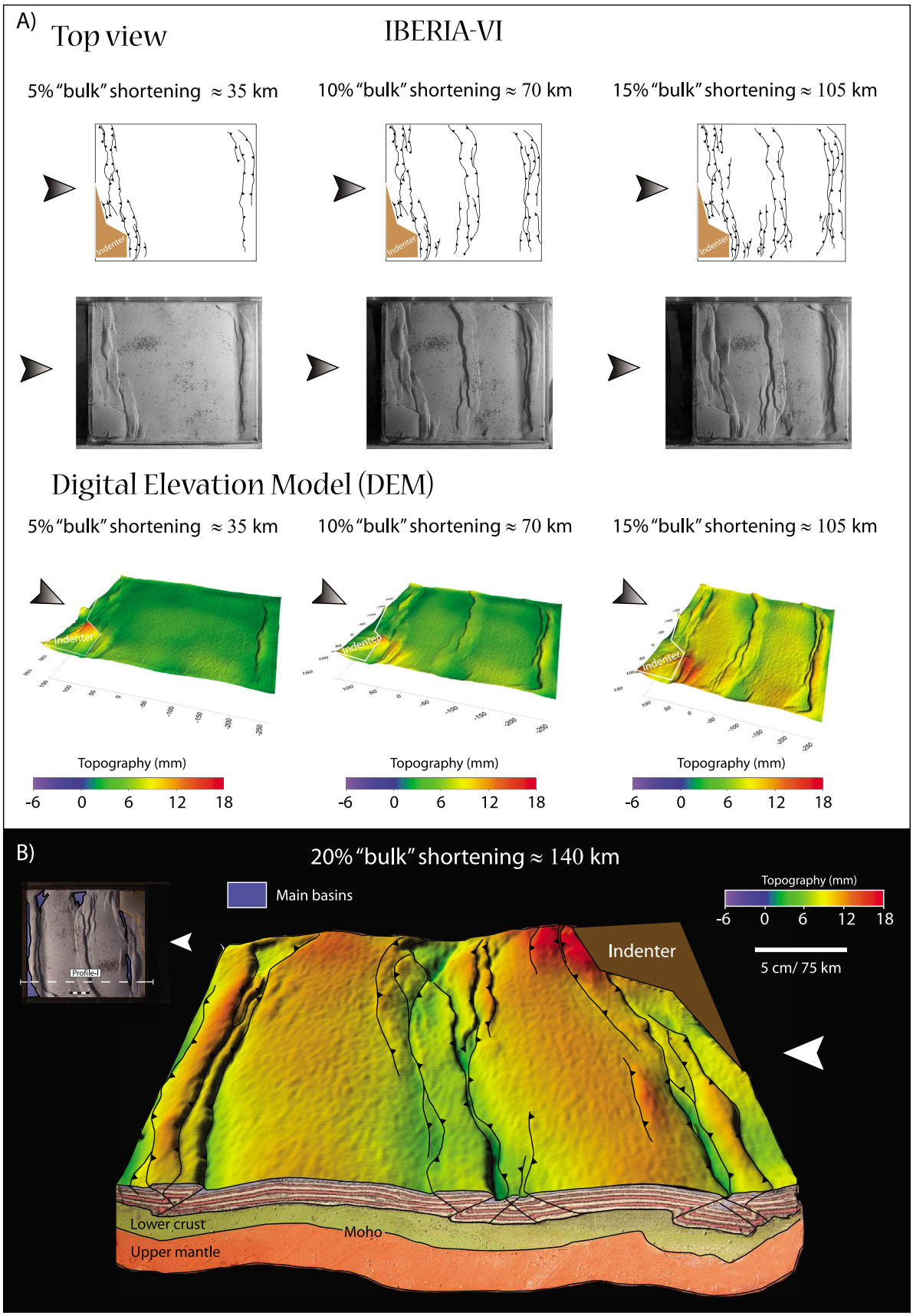

Figure 12

rheological stratification of the lithosphere. This fact has also been highlighted by analogue experiments of brittle-ductile systems [*Martinod and Davy*, 1992] and field observations [*Bonnet et al.*, 2000]. Our models concur with these results, showing an increase of wavelength for models with stronger upper lithosphere mantle (the wavelength for the strong lithosphere shown in Figure 11 is 250–300 km while for the weaker upper lithosphere mantle in Figure 12 it is around 150–225 km). Conversely, the change in the amplitude of the folding with the increase of velocity seems to be related to the distribution and localization of the deformation in the model. Distributed deformation promotes low amplitude whereas if it is more localized we observed higher amplitudes (see Figures 7, 8, 10 and 11).

[58] Despite the fact that our models do not address tectonic inversion or reactivation of preexisting crustal heterogeneities explicitly, comparison of the modeling results with natural intraplate settings is valid since these issues do not exert a first-order control on the deformation mechanism. In the following sections we will focus on a discussion of the modeling results in context of intraplate deformation in Iberia, yet comparison of our results with the crustal architecture of other intraplate settings such as the Eastern Cordillera in Columbia, the Atlas chain, or the Rocky Mountains argues for their relevance for those mountain belts as well.

7.3. Implications for Topography Development in Iberia

[59] From north to south, the relief of Iberia has been linked to processes of block rotation and uplift, inhomogeneous thickening of the lower crust or folding of the lithosphere [*Vegas et al.*, 1990; *Vergés and Fernández*, 2006; *Cloetingh et al.*, 2002; *De Vicente and Vegas*, 2009]. We describe the main topographic features as well as their related foreland basins in the context of folding of the Iberian lithosphere.

7.3.1. Cantabrian Mountains-Pyrenees Border

[60] The Cantabrian Mountains are the western prolongation of the Pyrenean belt in Iberia extending along 700 km from E to W. Together they form a mountain system with mean altitudes that reach 1000 and 2000 m, respectively. This high topography resulted from the oblique convergence and collision between the Iberian and European plates during most of the Cenozoic times. Geophysical data show northward subduction of the Iberian plate under Europe in the Pyrenees and complex lower crust geometries below the Cantabrian mountains, where European lower crust possible indented Iberian crust [*Derégnaucourt and Boillot*, 1982; *Pulgar et al.*, 1996; *Fernández-Viejo et al.*, 1998; *Pedreira et al.*, 2007].

[61] The northern continental margin of Iberia shows variations in crustal thicknesses from 30–32 km towards Galicia to 45–48 km below the Cantabrian Mountains and more than 50 km under the Pyrenees [*Gallastegui et al.*, 1997; *Fernández-Viejo et al.*, 1998; *Gallastegui*, 2000; *Pedreira et al.*, 2003; *Díaz and Gallart*, 2009].

[62] The Cantabrian Mountains are characterized by a basal detachment dipping towards the north between 15° and 18° and involve several thrust faults that place Paleozoic rocks on top of Cretaceous-Tertiary rocks and sediments of the Duero foreland basin [*Gallastegui*, 2000]. The result of a simultaneous interference of sedimentation, erosion, and tectonic uplift is portrayed by progressive unconformities and basinward thickness variations of strata that can be observed along the northern border of the Duero. Further east, the southern Pyrenean front is characterized by a series of antiformal stacks of thrusts that overlie Tertiary sediments of the Ebro foreland basin.

[63] Recent studies carried out by *Martín-González and Heredia* [2008] and *Martín-González* [2009] have provided new insight into the disappearance of E-W Pyrenean relief towards the south and the N-S to E-W distribution of Tertiary basins together with their connection with Alpine structures. As a result, a possible explanation proposed by *De Vicente and Vegas* [2009] involves the partitioning of the deformation through the left lateral deformation belts related to the Vilariça Fault System which ends in compressive step-overs that compensate the total shortening (Figure 1). In addition, fission track data show a complex cooling history from the Cretaceous to Tertiary times related to mountain building in that part of Iberia [*Martín-González et al.*, 2006].

[64] The experimental results allow constraining the effect of compression induced close to the collision border in the very beginning of the deformation. The resulting thickening of the lower crust and general uplift in the brittle upper part gives rise to the Northern mountain system by pop-ups and thrusting. The presence of an indenter localizes the strain leading to higher topography (compare models with and without indenter) and major thickening in the lower crust. A more realistic pattern in comparison with the natural prototype comes from models Iberia II and Iberia V, where thickening and obliquity of the system takes place close to the convergence area. At the same time, buckling is the overall process that affects the whole model.

[65] Lateral thickness variations affect mainly the ductile lower and at minor extent the upper lithospheric mantle. Subsequently, thickened areas correspond in general with areas where the crustal-mantle boundary suffers deflection, where the resultant topography is localized. This is clearly observed when we compare the vertical profile of the lithosphere below basins and mountain ranges (see Figures 7–13).

[66] Since the presence of the indenter is not sufficient to lead to partitioning of the deformation by thrusting and strike-slip faulting restricted to the northwestern border of the models, we anticipate that the western geometry in Iberia must be related to inherited structures in previously rifted crust that helped to transfer the deformation towards the

Figure 12. (a) Top view images from model Iberia VI; DEM images show the evolution of topography (see explanation in the text). (b) DEM shows general uplift of the model with two broad antiforms separating the main topographic features.

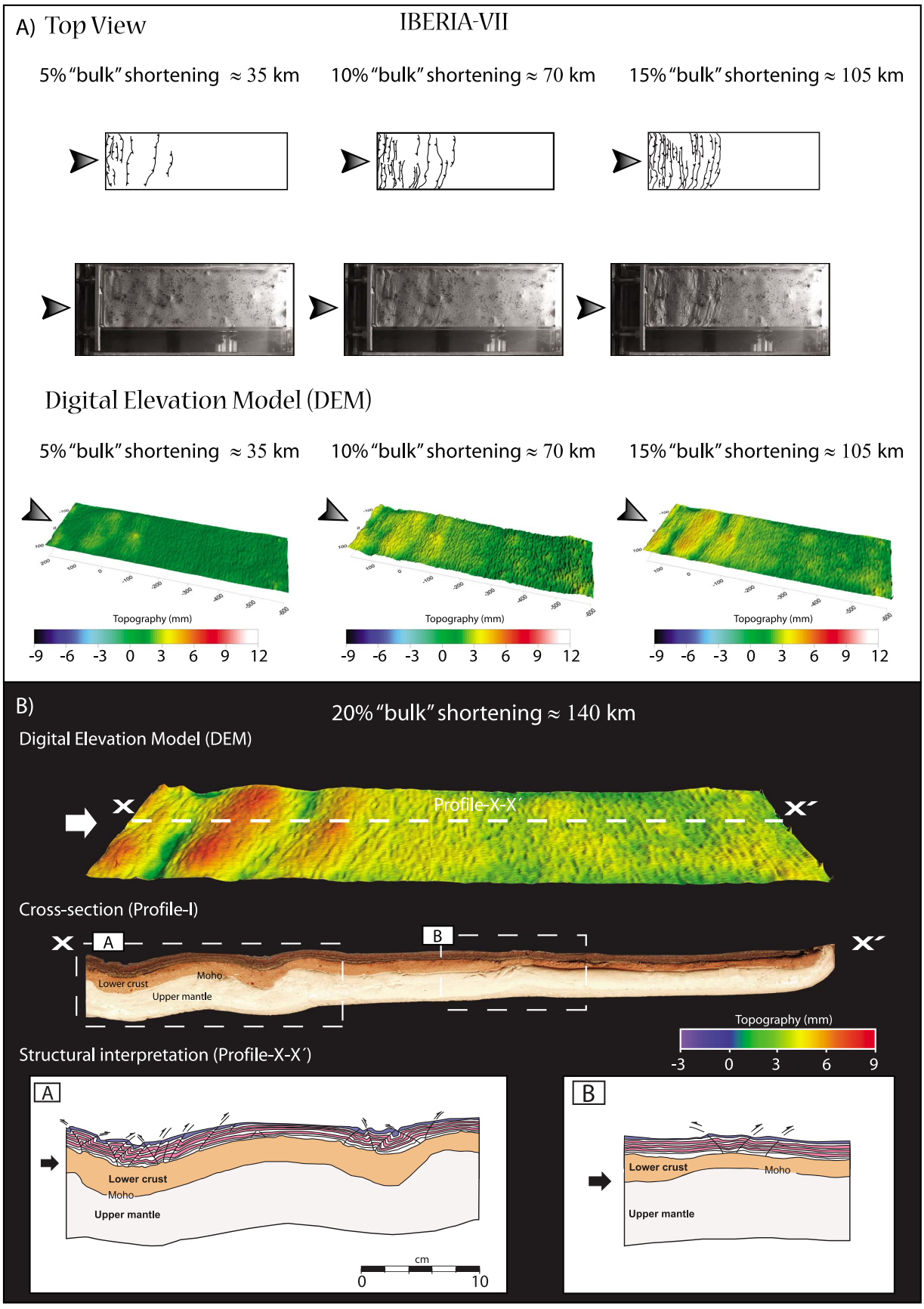

Figure 13

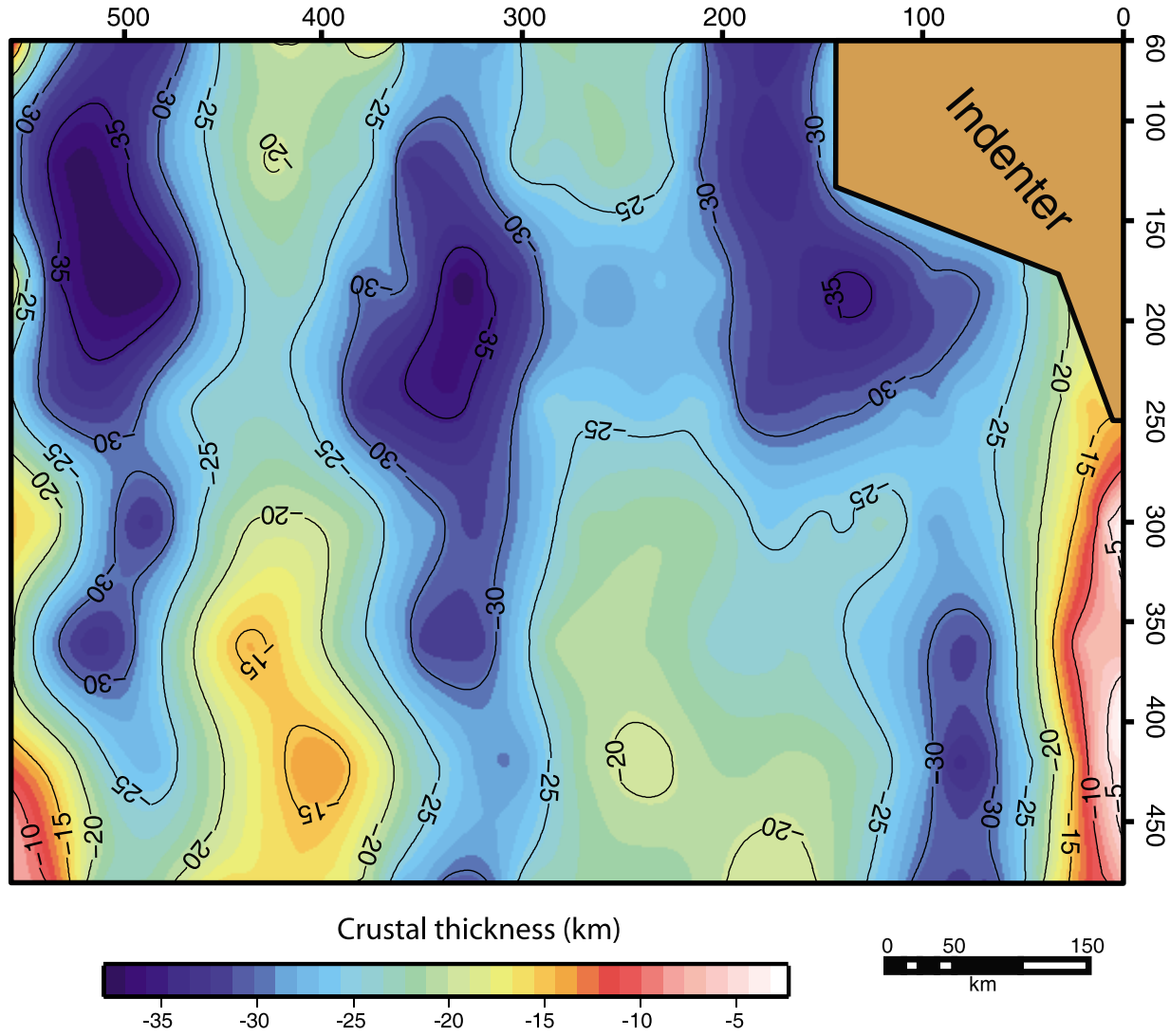

Figure 14. Isosurface of the Moho from model Iberia III, showing crustal thickness variations in response to buckling and the presence of an indenter, and active folding at the crust/mantle interface. Direction of compression from the right.

inner part of the microplate. Therefore, future experiments will examine the effect of subsequent weaker zones associated with rifting episodes since the Late Carboniferous-Early Permian times, during the unroofing of the Variscan orogen. Nevertheless, the indenter confined and localized structures with certain obliquity, localizing deformation in the northern part of the model. This mechanism has been proposed for the effect triggered by the opening of the King's Trough in the northern Atlantic margin of Iberia, which may affect on the final development and reactivation of structures along the western margin [*De Vicente and Vegas*, 2009].

7.3.2. Central Iberia

[67] Due to the lack of deep seismic data (wide angle reflexion and refraction profiles) little is known about the lithosphere structure in Central Spain. Despite the large amount of geological/structural data and gravity surveys, only the area of the Central System has been extensively studied [*De Vicente et al.*, 2007 and *Suriñach and Vegas*, 1988]. For this reason, we restrict out comparison to that mountain belt.

7.3.2.1. The Spanish Central System

[68] The Spanish Central System (SCS) constitutes a more than 700 km long mountain range extending from Portugal

Figure 13. (a) Structural interpretation of top view images and DEM from model Iberia VII (normal lithosphere under convergence rate of 0.5 cm h^{-1}). See text for further explanation. Arrows show the direction of convergence. (b) DEM shows general uplift of the model with three antiforms localized close to the moving wall (white arrow indicates direction of shortening). Profile along X-X′ and cross sections from insets a and b provide bases for structural interpretation.

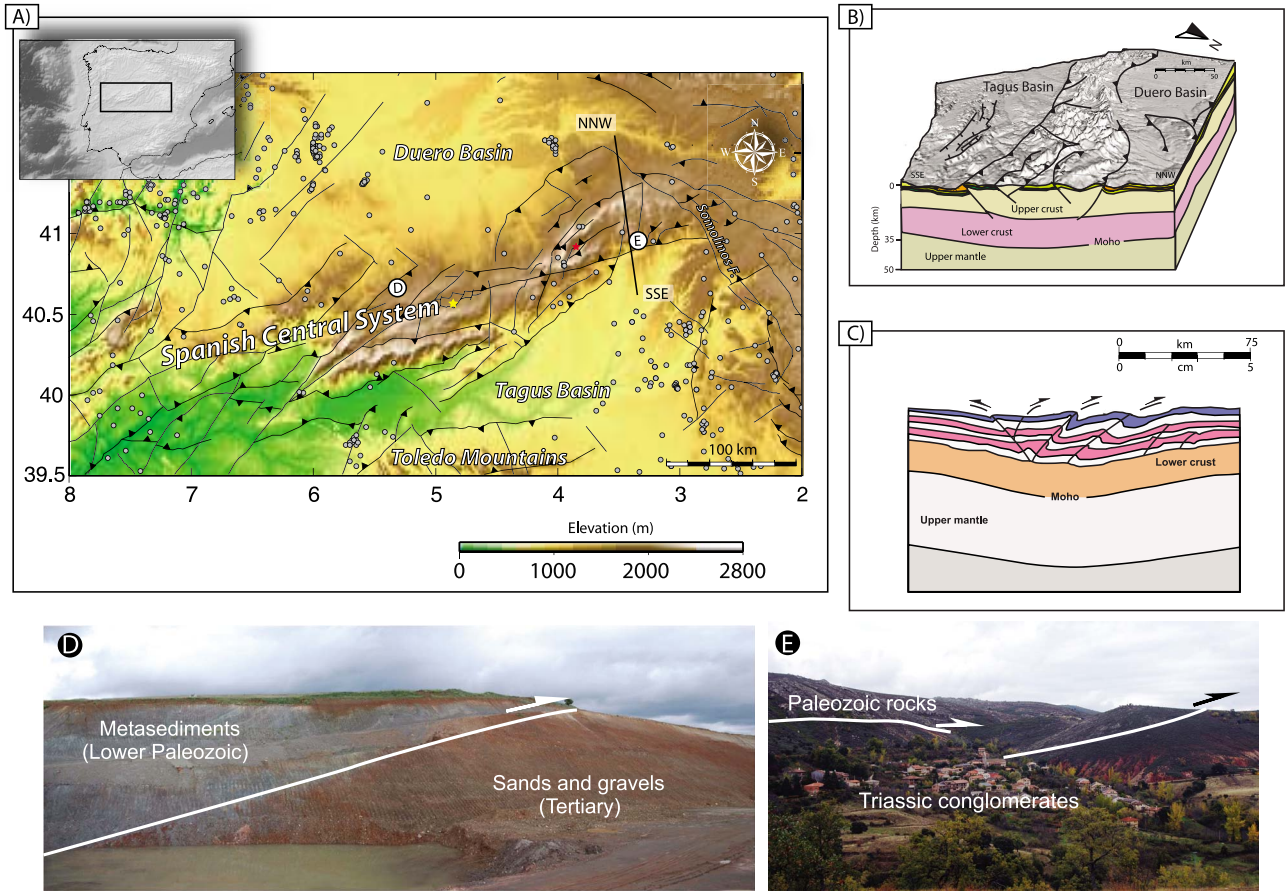

Figure 15. (a) Structural map of central Iberia. Stars show the position of (center) the Ambles and (upper right) Lozoya intramountain basins in the pop-downs. Seismicity data for 2008 provided by the Geographic National Institute of Spain. (b) Cross section along the NNW-SSE profile based on seismic data compiled by *Díaz and Gallart* [2009]. (c) Lithospheric-scale cross section of profile I of model Iberia IV. (d) Northern Border Fault (Avila, Spain) where Paleozoic metasediments overlay Tertiary sediments of the Duero Basin. (e) Southern Border Fault where Paleozoic rocks (Ordovician quartzite) are thrusted onto Triassic-Tertiary sediments of the Tagus Basin; southern thrust of the Spanish Central System at Almiruete (Guadalajara, Spain).

to Central Spain (Figure 1). It is defined as an asymmetric pop-up structure bordered to the north and south by the Duero and Tagus basins [*De Vicente et al.*, 2007]. Deep seismic profiling carried out by *Banda et al.* [1983] and *Suriñach and Vegas* [1988] show a crustal thickness of 32–35 km with thickening of the lower crust up to 5 km. Gravity modeling also supports this crustal architecture [*De Vicente et al.*, 2007]. The SCS is bordered by a northern and southern border fault, facing N and S, respectively. The northern border is mostly covered by sediments of the Duero basin. The southern thrust is more segmented involving Paleozoic, Mesozoic and Tertiary sediments. These faults juxtapose Variscan basement over Miocene fluvial sediments consisting of sandstones and conglomerates. Within the whole mountain system, series of pop-ups and pop-downs create space for intramountain basins filled with Tertiary sediments (Lozoya Basin, Amblés basin) (see Figure 15, insets a and b).

[69] Asymmetric uplift of the chain has been recorded by fission track data starting in the early Eocene in its western sector (Gredos Sierra) and late Miocene in the eastern part (Guadarrama sector) [*Andeweg et al.*, 1999; *De Bruijne and Andriessen*, 2002].

[70] Analogue models provide a lithospheric section consisting of a faulted upper crust that is uplifted by single thrust and pop-ups, a thickened ductile lower crust, and a folded lithospheric mantle. This relationship between crustal and mantle deformation and thickness variations across intraplate belts can explain the observed geometries within plate interiors. The SCS in central Spain serves as an example for such relationships, which are displayed in Figure 15b and are compared to our modeling results (Figure 15c). The mountain ranges coincide with the loci of the synclines of the buckle folds. Intramountain basins are developed between pop-ups.

[71] Inferences from modeling support the idea of relatively strong crust-mantle decoupling favoring SCS-type

structures. Pop-up structures nucleated at the brittle-ductile transition and propagate upward. Meanwhile ductile thickening becomes evident in the lower crust. The time span between the first observable thrust at the surface and the beginning of deformation in the central part leads to the conclusion that folding is involved in the mechanism that transfers deformation from the front towards the inner part of the model. Subsequently, intraplate deformation and thickening are related to both, thrusting and folding of brittle and ductile layers that compose the Iberian lithosphere. Unlikely, but in those models where crust-mantle coupling is strong, the lower crust is slightly thickened. Moreover, the pop-ups do not appear as common structures turning into imbricate thrust or single thrust. Differences in style of thrusting can be considered as resulting of crustal-mantle coupling.

[72] Observed similarities between models and nature led to the conclusion that higher convergence rates spread deformation faster. Hence in model Iberia II (convergence rate of 1 cm h^{-1}, see Table 1) the lag time from deformation close to the moving wall to propagation towards the interior of the model is relatively short, which is consistent with the temporal evolution of the SCS and Toledo Mountains as constrained by fission track analysis [*De Bruijne and Andriessen*, 2002; *Barbero et al.*, 2005]. Consequently, models Iberia I and Iberia V are probably the most plausible scenarios for a relatively stable lithosphere affected by shortening. Thickening of the lower crust is accompanied by thrusting on the upper most part of the crust (compare Figures 7 and 13). Later models are in agreement with data available in central Spain. Therefore, we propose folding for the entire lithosphere as a probable mechanism that could explain the topography and crustal structure of the SCS.

7.3.2.2. The Duero and Tagus Basins

[73] The Duero Basin is filled with more than 2500 m of sediments in its deepest part. In some places the sediments can be found at altitudes of 800 m. The Cenozoic (Paleocene in age?) fluvio-lacustrine sediments that fill the basin rest conformably on upper Cretaceous subtidal sediments that occupy the northern and eastern areas. Towards the west they lie unconformably on Variscan basement. In general these Cenozoic sediments represent advancing fan-delta systems [*Corrochano and Armenteros*, 1989]. In the eastern sector several folds have been mapped, explaining the differences of altitude and the incision produced by rivers where different erosion surfaces have been preserved from upper Oligocene [*Benito-Calvo and Pérez-Gonzalez*, 2007]. In addition, these authors recognized four erosion surfaces in the NE part of the Duero basin which have been related to different episodes of uplift affecting the basin. The emergence of the Iberian Range has been associated to the first erosion surface that affects Upper Cretaceous sediments and is defined by these authors in late Oligocene-early Miocene times, which coincides with the data provided by *Alonso-Gavilán et al.* [2004] based on evaporitic facies.

[74] Fault activity in the western and northern borders of the basin have been recognized during the middle Eocene marked by the propagation of alluvial fans towards the inner parts of the basin [*De Vicente et al.*, 2007, and references therein]. Towards the south, at the border with the SCS, the first sediments are of Eocene age producing thick sequences of alluvial fans.

[75] The Tagus Basin is located in the southern border of the SCS (Figure 1). It is filled with up to 3 km of Tertiary sediments and subdivided in small subbasins. A limited set of seismic reflection profiles provide restricted information available until now. The Mesozoic subtidal sediments display thickness variations from north to south. In contrast, Paleogene sediments appear disturbed by faulting and folding and an internal unconformity disrupt the lower Paleogene series which indicates tectonic activity already at that time. Moreover, a coarsening upward trend in the upper-middle Miocene sequence is interpreted to be related to its proximity to the Southern border fault [*De Vicente et al.*, 2007].

[76] Analogue experiments show two different sets of basins. Intermountain basins are in general wider and longer than intramountain basins and are situated in between mountain ranges. As shortening progresses these basins are uplifted and can become internally deformed, because they coincide with the location of the antiforms of the folded lower crust and upper mantle. The Duero Basin is an example of such an intermountain basin that is flanked by two mountain ranges and which is at remarkably high altitude (800 m).

[77] Intramountain basins appear to be associated with pop-downs, they are narrow and located between faults of the same mountain range. This is also observed in the SCS, where basins like the Ambles or Lozoya basin are developed within the main range as pop-downs. (Figure 15a). Consequently, the evolution of the basins follows two different evolutionary steps. First, convergence results in the development of basins associated with thrusting. Second, the latter basins are deformed internally by single thrust and blind reverse faults (see temporal evolution in Figures 7 and 8 producing internal uplift of the basins). This is clearly observed in the northern border of the Duero basin, where a progressive unconformity affecting Cretaceous to Paleocene sediments is developed during uplift and ongoing shortening.

8. Conclusions

[78] In this study the conditions which can explain the actual configuration of mountain ranges and basins in Iberia as a result of Cenozoic deformation are investigated. On the basis of the experimental work we conclude the following.

[79] 1. The first response to shortening is buckling of the whole lithosphere as a consequence of large-scale convergence. Similarities with Iberia suggest that lithospheric buckling is a viable mechanism controlling the E-W to NE-SW regular distribution of mountain ranges in Iberia. These results are compatible with geological and geophysical data from the SCS, Toledo Mountains, and Sierra Morena.

[80] 2. Long wavelength folding developed where the mantle is strong, or when the crust-mantle coupling was high, whereas shorter wavelengths are present when the mantle is weak even in cases when the lower crust is stronger than the mantle. As such the distribution of mountain ranges is related to the rheological stratification of

the lithosphere, which in the case of Iberia can be characterized as consisting of a ductile lower crust that is underlain by a stronger mantle lithosphere.

[81] 3. Buckling of the lithosphere is associated with thickening of the ductile layers, particularly when the layer is weak. Strong decoupling, therefore, favors flow of the ductile lower crust from the antiforms to the synforms resulting in significant thickness variations of the ductile lower crust.

[82] 4. The strength of the lower crust also influences the style of deformation in the brittle crust such that strong lower crust leads to asymmetric pop-ups, and duplexes in areas of localized deformation while a relatively weak lower crust preferentially leads to imbricated single thrusts or symmetric pop-ups.

[83] 5. The influence of the opening of the King's Trough, represented in the models by the presence of an indenter seems to be limited to affecting the orientation and spacing of thrusts within the upper crust. Its influence on the evolution and shape of structures is therefore limited to the western most margin of Iberia where it can be linked to the Cenozoic uplift of the Galicia Bank.

[84] 6. Our modeling results emphasize that formation, uplift, and internal deformation of intermountain basins like the Ebro or Duero Basins reflect a sequence of progressive deformation of the lithosphere, where early formed buckle folds are modified by other deformation mechanisms like thrusting in the upper crust and ductile flow in the lower crust during ongoing shortening.

[85] **Acknowledgments.** The study was supported by Consolider Ingenio 2006 Topo-Iberia CSD2006-00041, the Spanish National Research Program CGL2006-13926-C02-01-02 Topo-Iberia Foreland, and ISES, the Netherlands Research Centre for Integrated Solid Earth Sciences. The experiments were carried out at the Teclab of VU University in Amsterdam. The authors are very grateful to O. Oncken and two anonymous reviewers for their careful review and fruitful discussion which enriched this manuscript. Critical comments were provided by Stefan W. Luth. Endre Dombradi is thanked for his technical help at the Teclab. Helpful advice was also given by John Willmouth and Dave Green. The authors also want to thank Marious van Heiningen for showing some good outcrops in the field.

References

Alonso-Gavilán, G., I. Armenteros, J. Carballeira, A. Corrochano, P. Huerta, and J. M. Rodríguez (2004), Cuenca del Duero (Duero Basin), in *Geología de España*, edited by J. A. Vera, pp. 550–556, Soc. Geol. Esp., Inst. Geol. Minero Esp., Madrid, Spain.

Álvarez-Marrón, J., et al. (1996), Seismic structure of the northern continental margin of Spain from ESCIN deep seismic profiles, *Tectonophysics*, *264*, 153–174.

Anderson, E. M. (1951), *The Dynamics of Faulting*, 2nd ed., Oliver and Boyd, Edinburgh.

Andeweg, B., G. De Vicente, S. Cloetingh, J. L. Giner, and A. Muñoz-Martín (1999), Local stress fields and intraplate deformation of Iberia: Variations in spatial and temporal interplay of regional stress sources, *Tectonophysics*, *305*, 153–164.

Argus, D. F., R. G. Gordon, C. DeMets, and S. Stein (1989), Closure of the Africa-Eurasia-North America plate motion circuit and tectonics of the Gloria fault, *J. Geophys. Res.*, *94*(B5), 5585–5602, doi:10.1029/JB094iB05p05585.

Arthaud, F., and P. Matte (1977), Late Paleozoic strike-slip faulting in southern Europe and northern Africa: Result of a right-lateral shear zone between the Appalachians and the Urals, *Geol. Soc. Am. Bull.*, *88*, 1305–1320.

Banda, E., A. Udias, S. T. Mueller, J. Mezcua, M. Boloix, J. Gallart, and A. Aparicio (1983), Crustal structure beneath Spain from deep seismic sounding experiments, *Phys. Earth Planet. Inter.*, *31*, 277–280.

Banda, E., M. Comas, and D. Córdoba (1996), Seismic structure of the northern continental margin of Spain from ESCIN deep seismic profiles, *Tectonophysics*, *264*, 153–174.

Barbero, L., U. A. Glasmacher, C. Villaseca, J. A. López García, and C. Martín-Romera (2005), Long-term thermotectonic evolution of the Montes de Toledo area (Central Hercynian Belt, Spain): Constraints from apatite fission track analysis, *Inter. J. Earth Sci.*, *94*, 193–203.

Benito-Calvo, A., and A. Perez-Gonzalez (2007), Erosion surfaces and Neogene landscape evolution in the NE Duero Basin (north-central Spain), *Geomorphology*, *88*, 226–241.

Bird, P. (1991), Lateral extrusion of lower crust from under high topography in the isostatic limit, *J. Geophys. Res.*, *96*(B6), 10,275–10,286, doi:10.1029/91JB00370.

Bonnet, S., F. Guillocheau, J.-P. Brun, and J. Van Den Driessche (2000), Large-scale relief development related to Quaternary tectonic uplift of a Proterozoic-Paleozoic basement: The Armorican Massif, NW France, *J. Geophys. Res.*, *105*(B8), 19,273–19,288, doi:10.1029/2000JB900142.

Burg, J.-P., P. D. Nievergelt, F. Oberli, D. Seward, Z. Diao, and M. Meier (1997), Exhumation during crustal folding in the Namche-Barwa syntaxis, *Terra Nova*, *9*, 53–56.

Burov, E. B., and A. B. Watts (2006) The long-term strength of continental lithosphere: "Jelly sandwich" or "crème brûlée?", *GSA Today*, *16*, 4–10.

Burov, E., L. Lobkovsky, S. Cloetingh, and A. M. Nikishin (1993), Continental lithosphere folding in Central Asia, part II: Constraints from gravity and topography, *Tectonophysics*, *226*, 73–87.

Cann, J. R., and B. M. Funnell (1967), Palmer Ridge: A section through the upper part of the ocean crust?, *Nature*, *213*, 661–664.

Carbonell, R., et al. (2007), Seismic reflection transect across the Central Iberian Zone (Iberian Massif): The ALCUDIA Project, *EOS Trans. AGU*, *88*(52), Fall Meet. Suppl., Abstract T31B-0479.

Casas-Sainz, A. M., and G. de Vicente (2009), On the tectonic origin of Iberian topography, *Tectonophysics*, *474*, 214–235.

Choukroune, P., and ECORS Team (1989), The ECORS Pyrenean deep seismic profile. Reflection data and the overall structure of an orogenic belt, *Tectonics*, *8*(1), 23–39, doi:10.1029/TC008i001p00023.

Choukroune, P., F. Roure, B. Pinet, and ECORS Pyrenees Team (1990), Main results of the ECORS Pyrenees profile, *Tectonophysics*, *173*, 411–418.

Cloetingh, S., E. Burov, and A. Poliakov (1999), Lithosphere folding: Primary response to compression? (from central Asia to Paris Basin), *Tectonics*, *18*(6), 1064–1083, doi:10.1029/1999TC900040.

Cloetingh, S., E. Burov, F. Beekman, B. Andeweg, P. A. M. Andriessen, D. Garcia-Castellanos, G. De Vicente, and R. Vegas (2002), Lithospheric folding in Iberia, *Tectonics*, *21*(5), 1041, doi:10.1029/2001TC901031.

Corrochano, A., and I. Armenteros (1989), Los sistemas lacustres de la Cuenca terciaria del Duero (The lacustrine sedimentary systems of the Tertiary Duero Basin), *Acta. Geol. Hispanica*, *24*, 259–279.

Cortés, M., B. Colletta, and J. Angelier (2006), Structure and tectonics of the central segment of the Eastern Cordillera of Colombia, *J South Am. Earth Sci.*, *21*, 437–465.

Davy, P., and P. R. Cobbold (1991), Experiments on shortening of a 4-layer model of the continental lithosphere, *Tectonophysics*, *188*, 1–25.

De Bruijne, C. H., and P. A. M. Andriessen (2002), Far field effects of Alpine plate tectonism in the Iberian microplate recorded by fault-related denudation in the Spanish Central System, *Tectonophysics*, *349*, 161–184.

Del Río, P., L. Barbero, and F. Stuart (2006), Historia del levantamiento tectónico de la Sierra de Cameros (Cordillera Ibérica, España): Restricciones en base a cronología mediante huellas de fisión y (U-Th)/He en apatitos (History of the tectonic uplift of the Cameros Sierra (Iberian Chain, Spain): Constraints based on appatite fission track and (U-Th)/He), *Geogaceta*, *40*, 7–10.

Derégnaucourt, D., and G. Boillot (1982), Nouvelle carte structurale du Golfe de Gascogne, *C. R. Acad. Sci. Paris, Sér. II*, *294*, 219–222.

De Vicente, G., and R. Vegas (2009), Large-scale distributed deformation controlled topography along the western Africa-Eurasia limit: Tectonic constraints, *Tectonophysics*, *474*, 124–143.

De Vicente, G., J. L. Giner, A. Muñoz-Martín, J. M. González-Casado, and R. Lindo (1996), Determination of present day stress tensor and neotectonic interval in the Spanish Central System and Madrid Basin, central Spain, *Tectonophysics*, *266*, 405–424.

De Vicente, G., et al. (2007), Cenozoic thick-skinned deformation and topography evolution of the Spanish Central System, *Global Planet. Change*, *58*, 335–381.

De Vicente, G., et al. (2009), Oblique strain partitioning and transpression on an inverted rift: The Castilian Branch of the Iberian Chain, *Tectonophysics*, *470*, 224–242.

Díaz, J., and J. Gallart (2009), Crustal structure beneath the Iberian Peninsula and surrounding waters: A new compilation of deep seismic sounding results, *Phys. Earth Planet. Inter.*, *173*, 181–190.

Doglioni, C., F. Mongelli, and P. Fieri (1994), The Puglia uplift (SE Italy): An anomaly in the foreland of the Apenninic subduction due to buckling of a thick continental lithosphere, *Tectonics*, *13*, 1309–1321, doi:10.1029/94TC01501.

Fernàndez, M., and I. Marzán (1998), Heat flow, heat production, and lithospheric thermal regime in the Iberian Peninsula, *Tectonophysics*, *291*, 29–53.

Fernández-Viejo, G., J. Gallart, J. A. Pulgar, J. Gallastegui, J. Dañobeitia, and D. Córdoba (1998), Crustal transition between continental and oceanic domains along the North Iberian Margin from wide-angle seismic and gravity data, *Geophys. Res. Lett.*, *25*(23), 4249–4252, doi:10.1029/1998GL900149.

Gallastegui, J. (2000), Estructura cortical de la cordillera y margen continental cantábricos: Perfiles ESCI-N (Crustal structure of the Cantabiran mountains and its continental margin), *Trabajos de Geol.*, *22*, Univ. Oviedo, Oviedo, Spain.

Gallastegui, J., J. A. Pulgar, and J. Álvarez-Marrón (1997), 2-D seismic modelling of the Variscan foreland thrust and fold belt crust in NW Spain from ESCIN-1 deep seismic reflection data, *Tectonophysics*, *269*, 21–32.

Gerbault, M., E. Burov, A. Poliakov, and M. Daignières (1999), Do faults trigger folding in the lithosphere?, *Geophys. Res. Lett.*, *26*(2), 271–274, doi:10.1029/1998GL900293.

Guimerà, J., R. Salas, J. Vergés, and A. Casas (1996), Extensión mesozoica e inversión compresiva terciaria en la Cadena Ibeŕica: Aportaciones a partir del análisis de un perfil gravimetrico (Mesozoic extension and Tertiary compressional inversion in the Iberian chain: Insights from a gravity profile analysis), *Geogaceta*, *20*, 7697–7694.

Jackson, J. (2002), Faulting, flow, and the strength of the continental lithosphere, *Int. Geol. Rev.*, *44*, 39–61.

Jarosinski, M., F. Beekman, L. Matenco, and S. Cloetingh (2011), Mechanics of basin inversion: Finite element modelling of the Pannonian Basin System, *Tectonophysics*, in press.

Luth, S., E. Willingshofer, D. Sokoutis, and S. Cloetingh (2009), Analogue modeling of continental collision: Influence of plate coupling on mantle lithosphere subduction, crustal deformation, and surface topography, *Tectonophysics*, *484*, 87–102.

Martín-González, F. (2009), Cenozoic tectonic activity in a Variscan basement: Evidence from geomorphological markers and structural mapping (NW Iberian Massif), *Geomorphology*, *107*, 210–225.

Martín-González, F., and N. Heredia (2008), ¿Cómo finaliza la estructura de la Cordillera Cantábrico-Pirenaica hacia el Oeste?, *Geo-Temas*, *10*, 373–376.

Martín-Gónzález, F., R. Capote, L. Barbero, J. M. Insua, and J. J. Martínez-Díaz (2006), Primeros resultados de huellas de fisión en apatito en el sector Lugo-Ancares (Noroeste de la Península Ibérica) (First insights on apatite fission track analyses in the Lugo-Ancares sector (northwest of the Iberian Peninsula)), *Geogaceta*, *40*, 79–82.

Martinod, J., and P. Davy (1992), Periodic instabilities during compression or extension of the lithosphere 1: Deformation modes from an analytical perturbation method, *J. Geophys. Res.*, *97*(B2), 1999–2014, doi:10.1029/91JB02715.

Martín-Velázquez, S., G. de Vicente, and F. J. Elorza (2009), Intraplate stress state from finite element modeling: The southern border of the Spanish Central System, *Tectonophysics*, *473*, 417–427.

Márton, E., and M. C. Abranches (2004), Iberia in the Cretaceous: New paleomagnetic results from Portugal, *J. Geod*, *38*, 209–221.

Mattauer, M., and J. Henry (1974), Pyrenees, *Spec. Publ. Geol. Soc. London*, *4*, 3–21.

Mezcua, J., A. Gil, and R. Benarroch (1996), Estudio gravimetrico de la Peninsula Iberica y Baleares (Gravity survey of the Iberian Peninsula and Balearic Islands), *Inst. Geogr. Nac.*, 19 pp.

Minster, J., and T. Jordan (1978), Present-day plate motions, *J. Geophys. Res.*, *83*, 5331–5334.

Mulugeta, G. (1988), Squeeze-box in the centrifuge, *Tectonophysics*, *148*, 323–335.

Muñoz, J. A. (1992), Evolution of a continental collision belt: ECORS-Pyrenees crustal balanced cross-section, in *Thrust Tectonics*, edited by K. R. McClay, pp. 235–246, Chapman and Hall, London, U. K.

Muñoz-Martin, A., G. De Vicente, J. Fernandez-Lozano, S. Cloetingh, E. Willingshofer, D. Sokoutis, and F. Beekman (2011), Spectral analysis of the gravity and elevation along the western Africa-Eurasia plate tectonic limit: Continental versus oceanic lithospheric folding signals, *Tectonophysics*, in press.

Pedreira, D., J. A. Pulgar, J. Gallart, and J. Díaz (2003), Seismic evidence of Alpine crustal thickening and wedging from the western Pyrenees to the Cantabrian Mountains (North Iberia), *J. Geophys. Res.*, *108*(B4), 2204, doi:10.1029/2001JB001667.

Pedreira, D., J. A. Pulgar, J. Gallart, and M. Torné (2007), Three-dimensional gravity and magnetic modeling of crustal indentation and wedging in the western Pyrenees-Cantabrian Mountains, *J. Geophys. Res.*, *112*, B12405, doi:10.1029/2007JB005021.

Puigdefábregas, C., J. A. Muñoz, and J. Vergés (1981), in *Thrust Tectonics*, edited by K. R. McClay, pp. 235–246, Chapman and Hall, London, U. K.

Pulgar, J., J. Gallart, G. Fernández-Viejo, A. Pérez-Estaún, J. Álvarez-Marrón, and ESCIN Group (1996), Seismic image of the Cantabrian Mountains in the western extension of the Pyrenean belt from integrated reflection and refraction data, *Tectonophysics*, *264*, 1–19.

Ramberg, H. (1967), *Gravity*, *Deformation*, *and the Earth's Crust*, 224 pp., Academic, London, U. K.

Ramberg, H. (1981), *Gravity*, *Deformation*, *and the Earth*'s *Crust*, 2nd ed., 452 pp., Academic, London, U. K.

Rey, P., and O. Vanderhaeghe (2001), Gravitational collapse of the continental crust: Definition, regimes, and modes, *Tectonophysics*, *342*, 435–449.

Roca, E., O. Ferrer, N. Ellouz, B. Benjumea, J. A. Muñoz, and MARCONI Team (2008), The north Pyrenean Front and related foreland basin along the Bay of Biscay: Constraints from the MARCONI deep seismic reflection survey, *Geo-Temas*, *10*, 405–408.

Roure, F., P. Choukroune, X. Berasteguy, J. A. Muñoz, A. Villien, P. Matheron, M. Bareyt, M. Segurat, P. Camara, and J. Deramond (1989), ECORS deep seismic data and balanced cross sections: Geometric constraints to trace the evolution of the Pyrenees, *Tectonics*, *8*(1), 41–50, doi:10.1029/TC008i001p00041.

Ruiz, J., D. Gomez-Ortiz, and R. Tejero (2006), Effective elastic thicknesses of the lithosphere in the Central Iberian Peninsula from heat flow: Implications for the rheology of the continental lithospheric mantle, *J. Geodyn.*, *41*, 500–509.

Simancas, J. F., and R. Carbonell (2003), Crustal structure of the transpressional Variscan orogen of SW Iberia: SW Iberia deep seismic reflection profile (IBERSEIS), *Tectonics*, *22*(6), 1062, doi:10.1029/2002TC001479.

Sokoutis, D., M. Bonini, S. Medvedev, M. Boccaletti, C. J. Talbot, and H. Koyi (2000), Indentation of a continent with a built-in thickness change: Experiment and nature, *Tectonophysics*, *320*, 243–270.

Srivastava, S. P., W. R. Roest, L. C. Kovacs, G. Oakey, S. Lévesque, J. Verhoef, and R. Macnab (1990), Motion of Iberia since the Late Jurassic: Results from detailed aeromagnetic measurements in the Newfoundland Basin, *Tectonophysics*, *184*, 229–260.

Stephenson, R., B. Ricketts, S. Cloetingh, and F. Beekman (1990), Lithosphere folds in the Eurekan orogen, Arctic Canada?, *Geology*, *18*, 603–606.

Suriñach, E., and R. Vegas (1988), Lateral inhomogeneities of the Hercynian crust in central Spain, *Phys. Earth Planet. Inter.*, *51*, 226–234.

Teixell, A., M. L. Arboleya, M. Julivert, and M. Charroud (2003), Tectonic shortening and topography in the central High Atlas (Morocco), *Tectonics*, *22*(5), 1051, doi:10.1029/2002TC001460.

Tejero, R., and J. Ruiz (2002), Thermal and mechanical structure of the central Iberian Peninsula lithosphere, *Tectonophysics*, *350*, 49–62.

Tesauro, T., M. K. Kaban, S. Cloetingh, N. Hardebol, and F. Beekman (2007), 3D strength and gravity anomalies of the European lithosphere, *Earth Planet. Sci. Lett.*, *263*, 56–57.

Tesauro, M., M. K. Kaban, and S. Cloetingh (2008), EuCRUST-07: A new reference model for the European crust, *Geophys. Res. Lett.*, *35*, L05313, doi:10.1029/2007GL032244.

Tesauro, M., M. K. Kaban, and S. Cloetingh (2010), Thermal and rheological model of the European lithosphere, in *New Frontiers in Integrated Solid Earth Sciences*, edited by S. Cloetingh and J. Negendank, pp. 71–101, Springer, New York, doi:10.1007/978-90-481-2737-5_3.

Tikoff, B., and J. Maxson (2001), Lithospheric buckling of the Laramide foreland during Late Cretaceous and Paleogene, western United States, *Rocky Mt. Geol.*, *36*, 13–35.

Van Wees, J. D., and S. Cloetingh (1996), 3D flexure and intraplate compression in the North Sea Basin, *Tectonophysics*, *266*, 243–359.

Vegas, R. (2005), Alpine deformation of old massifs, The case of the Iberian Massif (Hesperic), *Bol. R. Soc. Esp. Hist. Nat., Secc. Geol.*, *100*, 39–54.

Vegas, R., J. Vázquez, E. Suriñach, and A. Marcos (1990), Model of distributed deformation, block rotations, and crustal thickening for the formation of the Spanish Central System, *Tectonophysics*, *184*, 367–378.

Vegas, R., T. Medialdea, and J. T. Vázquez (2008), Sobre la naturaleza del límite de placas actual entre la Península Ibérica y el norte de África, *Geo-Temas*, *10*, 1535–1538.

Vergés, J., and M. Fernández (2006), Ranges and basins in the Iberian Peninsula: Their contribution to the present topography, *Mem. Geol. Soc. Lond.*, *32*, 223–234, doi:10.1144/GSL.MEM.2006.032.01.13.

Weijermars, R. (1985), Flow behavior and physical chemistry of bouncing putties and related polymers in view of tectonic laboratory applications, *Tectonophysics*, *124*, 325–358.

Weijermars, R., and H. Schmeling (1986), Scaling of Newtonian and non-Newtonian fluid dynamics without inertia for quantitative modeling of rock flow due to gravity (including the concept of rheological similarity), *Phys. Earth and Planet. Inter.*, *43*, 316–330.

Willingshofer, E., and D. Sokoutis (2009), Decoupling along plate boundaries: Key variable controlling the mode of deformation and the geometry of collisional mountain belts, *Geology*, *37*, 39–42.

Willingshofer, E., D. Sokoutis, and J. P. Burg (2005), Lithospheric-scale analogue modeling of collision zones with a preexisting weak zone, *Geol. Soc. Spec. Publ.*, *243*, 277–294, doi:10.1144/GSL.SP.2005.243.01.18.

Ziegler, P. A., S. Cloetingh, and J. D. van Wees (1995), Dynamics of intraplate compressional deformation: The Alpine foreland and other examples, *Tectonophysics*, *252*, 7–22.

Ziegler, P., G. Bertotti, and S. Cloetingh (2002), Dynamic processes controlling foreland development: The role of mechanical (de) coupling of orogenic wedges and forelands, *Stephan Mueller Spec. Publ. Ser.*, *1*, 17–56.

S. Cloetingh, J. Fernández-Lozano, D. Sokoutis, and E. Willingshofer, Netherlands Research Centre for Integrated Solid Earth Science, Faculty of Earth and Life Sciences, VU University, De Boelelaan 1105, NL-1081 HV, Amsterdam, Netherlands. (javier.fernandez@falw.vu.nl)

G. De Vicente, Departamento de Geodinámica, F.C. Geológicas, Universidad Complutense de Madrid, Ciudad Universitaria, ES-28040, Madrid, Spain.